of the frequencies in Table I fails to reveal any such trend for any of the modes below 1000 cm^{-1}, in contrast to the porphyrin modes above 1450 cm^{-1}.[10,17,18] The band we identify with the lowest frequency A_{1g} mode, ν_9, ranges between 260 and 280 cm^{-1}, but there is no trend with the M–N distance (e.g., the $(Me_2SO)_2Fe^{III}$ frequency is higher than that of $(ImH)_2Fe^{III}$). Likewise the weak band near 230 cm^{-1}, which we assign to a B_{1g}, B_{2g}, or A_{2g} in-plane mode, shows a scatter of frequencies but no clear trend. Both of these bands are overlapped by the ~250-cm^{-1} pyrrole tilting mode, and their peak frequencies are difficult to determine reliably; it is conceivable that this uncertainty obscures an underlying trend. Nevertheless it is evident that the low-frequency RR spectra cannot readily be used as a monitor of the M–N(pyrrole) interaction.

Summary of Assignments

Because of the complexity of the low-frequency heme RR spectra, we illustrate in Figure 2 the assignments derived from this and previous[9] studies for NiPP and $(ImH)_2Fe^{II}PP$.

1. 1010–575 cm^{-1}. This region contains a number of in-plane porphyrin skeletal modes, which can readily be correlated with RR or IR modes of NiOEP. Several E_u modes are activated via the asymmetrically disposed vinyl groups of PP. In addition two out-of-plane hydrogenic modes are observed for $(ImH)_2Fe^{II}PP$: $\gamma_{CH=}$(vinyl) at 1008 cm^{-1} and γ_{C_mH} at 841 cm^{-1}.

2. 510–425 cm^{-1}. No in-plane modes occur in this region, but pyrrole folding modes are activated in $(ImH)_2Fe^{II}PP$ and in other iron complexes. Specific protein activation is seen for Mb derivatives.

3. 425–290 cm^{-1}. This region contains a cluster of bands of different types and of variable intensities in different complexes. The most prominent feature is usually the in-plane skeletal mode, ν_8, at ~345 cm^{-1}. It is usually accompanied by a mode at ~370 cm^{-1}, believed to be $2\nu_{35}$, in Fermi resonance with ν_8. At about the same frequency, however, is an out-of-plane mode, assigned here as γ_{C_bS}, coupled to the pyrrole folding mode at ~250 cm^{-1}, as evidenced by its ^{54}Fe shift. There are two flanking bands in PP complexes, assigned to vinyl bending modes, $\delta_{C_bC_aC_{\beta(1and2)}}$, at ~415 and ~320 cm^{-1}. Near, the latter band, at ~300 cm^{-1}, is another out-of-plane mode, $\gamma_{C_aC_m}$, involving the methine carbon atoms primarily.

4. 275–220 cm^{-1}. This region contains a cluster of at least three bands. In the middle, at ~250 cm^{-1}, is a ^{54}Fe- and ^{15}N(pyrrole)-sensitive band, assigned to pyrrole tilting. On either side, at ~260 and ~230 cm^{-1}, are bands assigned to in-plane skeletal modes, the higher of which is probably $\nu_9(A_g)$. While these bands can be expected to have some contribution from M–N stretching, their frequencies do no appear to correlate with the M–pyrrole distances.

Acknowledgment. This work was supported by NIH Grant HL 12526. We are indebted to Professor K. M. Smith for provision of vinyl-deuterated heme (supported by NIH Grant HL 22252) and to Professor G. N. La Mar for provision of Mb reconstituted with vinyl-deuterated heme (supported by NIH Grant HL 16087).

Registry No. $(ImH)_2Fe^{II}PP$, 85293-61-4; $(ImH)_2{}^{54}Fe^{II}PP$, 85282-43-5; $[(ImH)_2Fe^{III}OEP]Cl$, 85282-40-2; $[(ImH)_2{}^{54}Fe^{III}OEP]Cl$, 85293-64-7; $K[(CN)_2Fe^{IV}OEP]$, 85282-42-4; (2-MeImH)$Fe^{II}PP$, 85282-39-9; (2-MeImH)$^{54}Fe^{II}PP$, 85304-54-7; $ClFe^{III}PP$, 84009-29-0; $[(CN)_2Fe^{II}PP]^{2-}$, 85282-38-8; $[(CN)_2{}^{54}Fe^{II}PP]^{2-}$, 85304-53-6; NiPP, 85282-41-3.

(42) Hoard, J. L.; Scheidt, W. R. *Proc. Natl. Acad. Sci. U.S.A.* **1973**, *70*, 3919; **1974**, *70*, 1578.

Resonance Raman and Electronic Spectra of Heme *a* Complexes and Cytochrome Oxidase

S. Choi,[†] J. J. Lee,[‡] Y. H. Wei,[‡] and T. G. Spiro*[†]

Contribution from the Chemistry Departments, Princeton University, Princeton, New Jersey 08544, and State University of New York, Albany, New York 12222.
Received August 2, 1982

Abstract: Resonance Raman (RR) spectra of heme *a* complexes containing Fe^{II} and Fe^{III} in low- and high-spin states are assigned by comparison with protoheme analogues and by deuteration of the formyl substituent. Specific effects of the trans-conjugated formyl and vinyl groups include (a) RR enhancement of formyl and vinyl modes, (b) *x,y* splitting of the Q absorption bands by ~1600 cm^{-1}, (c) depolarization ratios near $^1/_3$ for most RR bands, (d) RR activation, and splitting, of E_u skeletal modes, with selective enhancements of the *x*- and *y*-polarized components, (e) skeletal mode shifts associated with the stabilization of one of the alternative 18-membered delocalization pathways of the porphyrin π system. For $(ImH)_2Fe^{II}Pa$ (ImH = imidazole, P*a* = porphyrin *a*), increased Q-band splitting (~2000 cm^{-1}) and skeletal mode shifts are attributed to $d_\pi \rightarrow$ porphyrin π^* back-bonding; the formyl C=O stretching frequency is also lowered in this complex. For all complexes, the C=O frequency is lower in aqueous than in nonaqueous solutions, due to formyl H bonding. The skeletal frequencies above 1450 cm^{-1} correlate with porphyrin core size, as they do for protoheme complexes, and with the same slopes. Heme *a* aggregates in aqueous solution show no RR frequency changes, beyond the effects of H bonding, but display altered intensity patterns, attributable to the absorption wavelength changes and to altered excited-state distortions; striking intensity changes are seen for low-frequency bands assigned to out-of-plane deformations. The 4131-Å RR spectrum of oxidized cytochrome oxidase is dominated by heme a_3 while the 4545-Å spectrum of the reduced protein is dominated by heme *a*, although contributions from the remaining heme can be seen. In the oxidized form, the low-frequency RR spectrum is interpreted in terms of heme a_3 perturbed by protein–peripheral substituent interactions, instead of Cu^{2+} vibrations, as recently suggested; the heme a_3 skeletal frequencies are consistent with EXAFS results, indicating a long bond to the sixth ligand.

RR spectroscopy is being increasingly applied as a structure probe for heme proteins.[1] Cytochrome oxidase is an attractive subject for RR studies, and a number of spectra have been published[2-11] and discussed since the early report by Salmeen et al.[2] The protein complex contains two heme *a* molecules and two

[†] Princeton University.
[‡] State University of New York.

(1) Spiro, T. G. In "The Chemical Physics of Biologically Important Inorganic Choromophores"; Lever, A. B. P., Gray, H. B., Eds.; Addison-Wesley: Reading, MA, in press.

0002-7863/83/1505-3692$01.50/0

Cu atoms. All of these metal centers occur in distinctly different environments, and the enzyme can be prepared in a variety of oxidation and ligation states, giving complex spectra.[12] One of the hemes, labeled a_3 is accessible to exogenous ligands and, in the native oxidized state, is spin-coupled to one of the Cu^{2+} ions, probably via a bridging sulfur atom of a cysteine ligand.[13] The other heme, labeled *a*, is magnetically isolated and is always in a low-spin state, presumably maintained by a pair of endogenous strong field ligands, e.g., imidazole.

The RR spectra of cytochrome oxidase have been attributed to the heme groups, although Woodruff et al.[10] have suggested that the Cu–ligand vibrations may be observable in the low-frequency region. A major problem for spectral interpretation is to disentangle the separate contributions of the two heme groups. To some extent this can be accomplished by judicious selection of the laser wavelength, taking advantage of differences in the absorption spectra associated with the different heme oxidation and ligation states.[8-11]

Some RR data on isolated heme *a* complexes have been reported,[3,9,11] but a more thoroughgoing analysis of the heme *a* vibrational spectrum is needed to permit RR spectroscopy of cytochrome oxidase to reach its full potential. Toward this end, we have undertaken to assign the skeletal and peripheral modes of heme *a*, with the aid of correlations to the recently assigned modes of protoporphyrin,[14-16] using both RR and IR spectroscopy. Frequency–structure correlations have been obtained for several representative heme *a* complexes, and solvent effects on the formyl C=O stretching frequency and on the intensity of porphyrin out-of-plane modes have been investigated. RR spectra of cytochrome oxidase, in oxidized and reduced forms, have been interpreted on the basis of these assignments.

Experimental Section

Cytochrome oxidase was prepared by the method of Okunuki et al.,[17] in 0.05 M phosphate buffer, pH 7.4, containing 1% of the detergent Brij-35. Heme *a* was extracted from purified oxidase, as the chloride complex.[18] The isolated heme *a* was dried and stored under Ar in a freezer. Samples of $ClFe^{III}Pa$ (Pa is the heme *a* porphyrin) were prepared by dissolving heme *a* chloride in CH_2Cl_2. The $[(Me_2SO)_2Fe^{III}Pa]^+$ complex was prepared by dissolving heme *a* chloride in Me_2SO; the Me_2SO is known to displace the bound chloride.[15] Samples of $[(ImH)_2Fe^{III}Pa]^+$ (ImH = imidazole) were prepared by adding excess imidazole to solutions of heme *a* chloride in CH_2Cl_2 or Me_2SO, or in H_2O (after dissolution in a small amount of 0.1 M NaOH) with or without 2% Brig-35. $(ImH)_2Fe^{II}Pa$ was prepared by reducing the $[(ImH)_2Fe^{III}Pa]^+$ solutions with a minimum amount (determined from the product absorption spectrum) of sodium dithionite, under Ar gas. For nonaqueous solutions, 18-crown-6 (Eastman) was added to solubilize the dithionite.[20] $(2\text{-MeImH})Fe^{II}Pa$ (2-MeImH = 2-methylimidazole) was prepared by adding excess 2-MeImH to heme *a* chloride solutions and reducing with dithionite. Absorption spectra were recorded in all cases.

Dueterium exchange for the formyl proton was carried out in alkaline D_2O containing KCN.[21] Solid KCN (5-fold molar excess) was added to an alkaline (pD 11) D_2O solution of $[(ImH)_2Fe^{III}Pa]^+$, and the solution was stored at 4 °C for a week. The progress of the exchange reaction was monitored via the RR spectrum (see Discussion). This solution was reduced with dithionite to obtain a sample of formyl-deuterated $(ImH)_2Fe^{II}Pa$.

RR spectra were obtained via backscattering (135°) from a spinning NMR sample tube, cooled with cold N_2 gas, and collected with a SPEX 1401 double monochromator equipped with a cooled photomultiplier (RCA) and photon-counting electronics, under computer (MINC) control. The spectra were smoothed with a Fourier filter. Excitation was provided by various Kr^+ and Ar^+ laser (Spectra Physics 170, 171) lines and by an Ar^+-pumped dye (Rhodamine 6G) laser (Coherent Radiation Model 590).

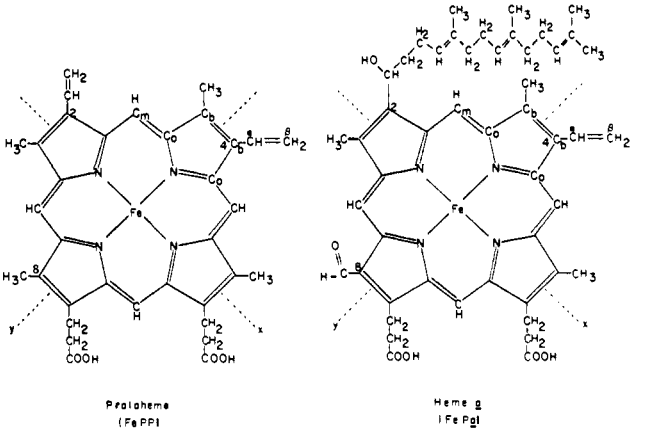

Figure 1. Molecular structure of protoheme and heme *a*; *x* and *y* denote the pseudo-symmetry axes.

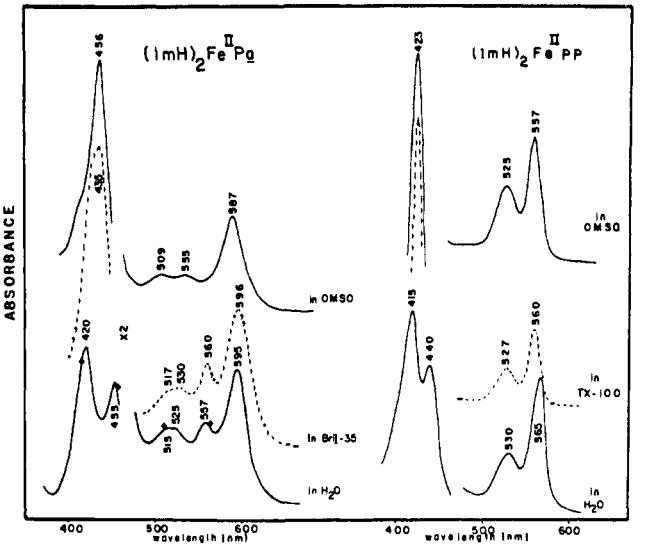

Figure 2. Absorption spectra of $(ImH)_2Fe^{II}Pa$ (left side) and of $(ImH)_2Fe^{II}PP$ (right side) in Me_2SO, H_2O, and aqueous detergent (Brij-35).

Results and Discussion

A. Heme *a* Electronic Structure. Heme *a* has the basic porphyrin 26-electron π system, but also has conjugated vinyl and

(2) Salmeen, I.; Rimai, L.; Gill, D.; Yamamoto, T.; Palmer, G.; Hartzell, C. R.; Beinert, H. *Biochem. Biophys. Res. Commun.* **1973**, *52*, 1100–1107.
(3) Kitagawa, T.; Kyogoku, Y.; Orii, Y. *Arch. Biochem. Biophys.* **1977**, *181*, 228–235.
(4) (a) Salmeen, I.; Rimai, L.; Babcock, G. *Biochemistry* **1978**, *17*, 800. (b) Babcock, G. T.; Salmeen, I. *Biochemistry* **1979**, *18*, 2493.
(5) Adar, F.; Yonetani, T. *Biochim. Biophys. Acta* **1978**, *502*, 80–86.
(6) Ondrias, M. R.; Babcock, G. T. *Biochem. Biophys. Res. Commun.* **1980**, *93*, 29–35.
(7) Bocian, D. F.; Lemley, A. T.; Petersen, N. O.; Brudvig, G. W.; Chan, S. I. *Biochemistry* **1979**, *18*, 4396.
(8) Woodruff, W. H.; Dallinger, R. F.; Antalis, T. M.; Palmer, G. *Biochemistry* **1981**, *20*, 1332–1338.
(9) (a) Callahan, P. M.; Babcock, G. T. *Biochemistry* **1981**, *20*, 952. (b) Babcock, G. T.; Callahan, P. M.; Ondrias, M. R.; Salmeen, I. *Ibid.* **1981**, *20*, 952–966.
(10) Woodruff, W. H.; Kessler, R. H.; Ferris, N. S.; Dallinger, R. F.; Carter, K. R.; Antalis, T. M.; Palmer, G. *Adv. Chem. Ser.*, in press.
(11) Steelandt-Frentrup, J. V.; Salmeen, I.; Babcock, G. T. *J. Am. Chem. Soc.* **1981**, *103*, 591–592.
(12) Malmstom, B. G. In "Metal Ion Activation of Dioxygen"; Spiro, T. G., Ed.; Wiley: New York, 1980, pp 181–208.
(13) Powers, L.; Chance, B.; Cheng, Y.; Angiolillo, P. *Biophys. J.* **1981**, *34*, 465–498.
(14) Choi, S.; Spiro, T. G.; Langry, K. C.; Smith, K. N. *J. Am. Chem. Soc.* **1982**, *104*, 4337–4344.
(15) Choi, S.; Spiro, T. G.; Langry, K. C.; Smith, K. N.; Budd, D. L.; La Mar, G. N. *J. Am. Chem. Soc.* **1982**, *104*, 4345–4351.
(16) Choi, S.; Spiro, T. G. *J. Am. Chem. Soc.*, preceding paper in this issue.
(17) Okunuki, K.; Sekuzu, I.; Yonatoni, T.; Kakemori, S. *J. Biochem. (Tokyo)* **1958**, *45*, 847–854.
(18) Takemori, S.; King, T. E. *J. Biol. Chem.* **1965**, *240*, 504–513.
(19) Hoard, J. L.; Scheidt, W. R. *Proc. Natl. Acad. Sci U.S.A.* **1973**, *70*, 3919; **1974**, *70*, 1578.
(20) Mincey, T.; Traylor, T. G. *Bioinorg. Chem.* **1978**, *9*, 409–420.
(21) Chancellor, T.; Quill, M.; Bergbreiter, E.; Newcomb, M. *J. Org. Chem.* **1978**, *43*, 1245–1246.

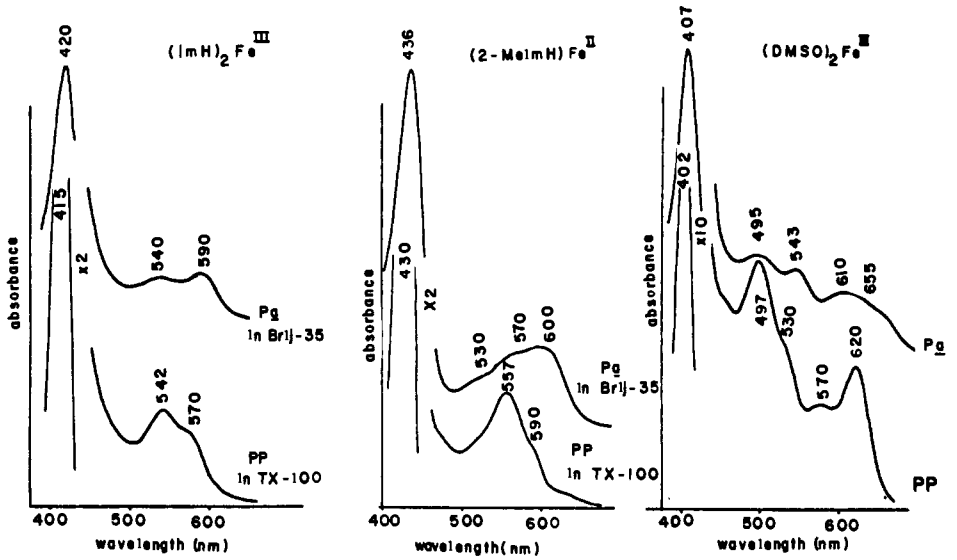

Figure 3. Absorption spectra of the indicated complexes of heme *a* (top) and protoporphyrin (bottom), in aqueous detergent, or (last panel) Me_2SO.

formyl peripheral substituents at positions 2 and 8, trans to each other across the porphyrin ring (Figure 1). Because of this trans disposition, the 18-membered aromatic pathway involving the vinyl- and formyl-bearing pyrrole rings is extended, whereas the alternate pathway involving the other pair of pyrrole rings is not. This conjugation pattern is expected to lead to a splitting of the *x*- and *y*-polarized components of the otherwise degenerate (E_u in D_{4h} symmetry) electronic transitions.[22] The situation is different for protoporphyrin (Figure 1), with conjugated substituents at the 2- and 4-positions. These positions are cis, with respect to the porphyrin ring, and the substituents affect the two 18-membered conjugation pathways equally. The *x* and *y* electronic transitions remain degenerate, even though the actual molecular symmetry is only C_s. Some of the consequences of this difference for heme *a* RR scattering have been discussed by Woodruff et al.[10]

The extent of the *x,y* splitting in heme *a* has not previously been determined, to our knowledge. Figure 2 gives evidence that this splitting is on the order of 2000 cm^{-1} in $(ImH)_2Fe^{II}Pa$ (P*a* is the porphyrin of heme *a*). In water, this complex shows four distinct absorption bands in the 500–600-nm region, while the protophorphyrin analogue, $(ImH)_2Fe^{II}PP$, shows only two, at 565 and 530 nm (Figure 2). The latter are understood[22] to be the Q_0 and Q_1 components of the lowest degenerate $\pi-\pi^*$ transition; the Q_1 band is the envelope of 0–1 vibronic levels, and its separation from the Q_0 frequency, 1170 cm^{-1}, represents an intensity-weighted average of the vibronically active modes. The four-banded spectrum of $(ImH)_2Fe^{II}Pa$ is reminiscent of the spectrum of free-base porphyrins,[22] in which protonation of two pyrrole rings splits the electronic degeneracy and produces pairs of absorption bands arising from the 0–0 and 0–1 components of the separate Q_x and Q_y transitions. We assign the most intense $(ImH)_2Fe^{II}Pa$ band, at 595 nm to Q_{y0}, polarized along the formyl–vinyl vector (Figure 1); Babcock et al.[23] found the Q/B oscillator strength ratio to be about 3 times higher for heme *a* than for protoheme; it seems reasonable to attribute this enhancement specifically to the transition involving the formyl–vinyl conjugation. The weaker band at 525 nm is assigned to Q_{x0}, leaving the 557 and 515 nm bands as Q_{y1} and Q_{x1}. This assignment implies an *x*–*y* splitting of 2200 cm^{-1}. The alternative assignment of the 557-nm band to Q_{x0} and the 525- and 515-nm bands to Q_{y1} and Q_{x1} is excluded because the 2200-cm^{-1} separation between the 595- and 525-nm bands, which would then be the Q_y 0–1 interval, is greater than any of the vibronically active frequencies, which are known from RR spectroscopy to extend only to 1670 cm^{-1} for heme *a* complexes.

It can be excluded that the 557-nm band is due to dithionite reduction of the formyl group[24] leaving a mono-vinyl heme. In view of the 3 times lower Q/B ratio expected[23] for such a heme (which is in approximate agreement with the ratio actually observed upon formyl reduction with excess dithionite[24]), it should exhibit a prominent B band, at 420 nm.[24] This is clearly absent in the detergent sample (Figure 2). The aqueous solution does show a 420-nm band, but this is due to the aggregation-induced[25] B-band splitting. Positive evidence that the aqueous 557-nm band is due to unaltered heme *a*, is provided by the RR spectrum with 5682-Å excitation, which shows strong enhancement of a skeletal mode, ν_{10}, at 1504 cm^{-1}, an anomalously low-frequency characteristic of $(ImH)_2Fe^{II}Pa$ (vide infra).

The apparent 0–1 separations in heme absorption spectra are variable, because they represent weighted averages of vibronic frequencies that are subject to subtle environmental effects. This is evident from a comparison (Figure 2) of the $(ImH)_2Fe^{II}Pa$ spectrum in water, detergent dispersion (Brij-35) and Me_2SO. Addition of detergent disperses the aqueous aggregates and collapses the B band; the Q-band pattern remains the same. In Me_2SO the relative 0–1 separations are reversed: the Q_{x0} and Q_{x1} bands (535 and 509 nm) are now 950 cm^{-1} apart, while the Q_{y0} and Q_{y1} bands have merged into a single band, 587 nm, which is significantly broader than the Q_0 band of $(ImH)_2Fe^{II}PP$ (Figure 2) (1008 cm^{-1} vs 650 cm^{-1} width at half-height).

The spectrum of $[(ImH)_2Fe^{III}Pa]^+$ (Figure 3) shows only two bands in the visible region, as does $[(ImH)_2Fe^{III}PP]^+$. The bands of the latter are broad, presumably reflecting rapid electronic deexcitation[26] associated with the d_π vacancy in low-spin Fe^{III}; the apparent 0–1 interval is only 850 cm^{-1}. For $[(ImH)_2Fe^{III}Pa]^+$ the separation of the two absorption bands is much larger, 1570 cm^{-1}; while this is within the range of vibronic frequencies, it probably represents the *x,y* splitting, with the 0–1 components being merged in the broadened absorptions. Similar evidence for *x,y* splitting can be seen in the broadened spectrum of the five-coordinate Fe^{II} complex, $(2\text{-MeImH})Fe^{II}Pa$, relative to $(2\text{-MeImH})Fe^{II}PP$ (Figure 3). The absorption spectra of high-spin Fe^{III} hemes are complicated by charge-transfer contributions[22] but extra broadening for $[(Me_2SO)_2Fe^{III}Pa]^+$ relative to $[(Me_2SO)_2Fe^{III}PP]^+$ (Figure 3) is again evidence for *x,y* splitting.

Thus, it appears that heme *a* shows an intrinsic ~1600-cm^{-1} *x,y* splitting of its lowest $\pi-\pi^*$ transitions. The low-spin bis-

(22) Gouterman, M. In "The Porphyrins"; Dolphin, D., Ed.; Academic Press: New York, 1979; Vol. III, Part A, pp 1–156.
(23) Babcock, G. T.; Ondrias, M. R.; Gobeli, D. A.; Vansteelandt, J.; Leroi, G. E. *FEBS Lett.* **1979**, *108*, 147–151.
(24) Vanderkooi, G.; Stotz, E. *J. Biol. Chem.* **1965**, *240*, 3418–3424.
(25) (a) Vanderkooi, G.; Stotz, L. *J. Biol. Chem.* **1966**, *241*, 2260–2267. (b) Gallagher, W. A.; Elliott, W. B. *Ann. N.Y. Acad. Sci.* **1973**, *206*, 463–482.
(26) Adar, F.; Gouterman, M.; Aronowitz, S. *J. Phys. Chem.* **1976**, *80*, 2184.

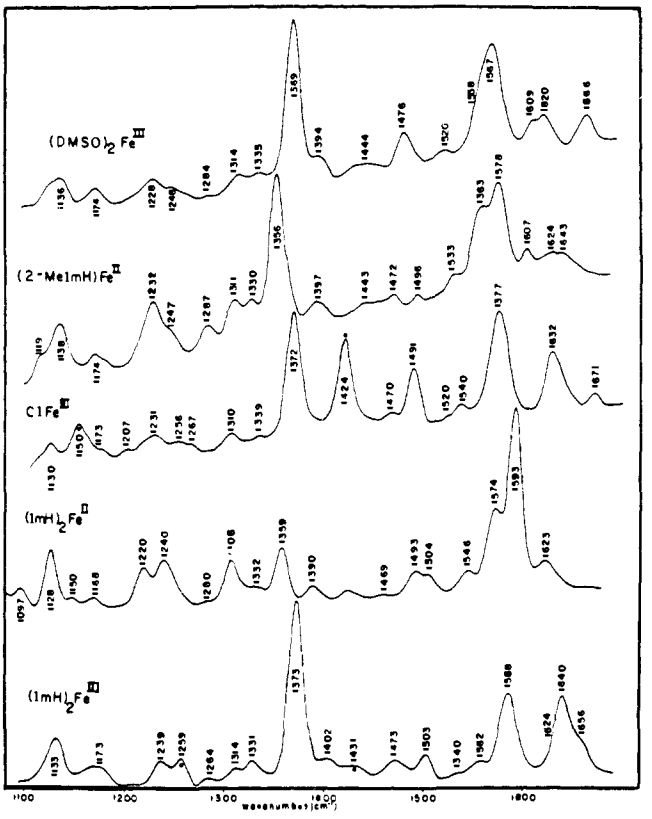

Figure 4. RR spectra, above 1000 cm^{-1}, with B-band excitation, for $[(Me_2SO)_2Fe^{III}Pa]^+$ in Me_2SO-d_6, λ_0 = 4131 Å; (2-MeImH)$Fe^{II}Pa$ in aqueous Brij-35 (2%), λ_0 = 4545 Å; Cl$Fe^{III}Pa$ in CH_2Cl_2, λ_0 = 4131 Å; $(ImH)_2Fe^{II}Pa$ in H_2O, λ_0 = 4579 Å; $[(ImH)_2Fe^{III}Pa]^+$ in H_2O, λ_0 = 4131 Å. Conditions: 100-mW laser power, 10-cm^{-1} slit width, 2 s/0.5 cm^{-1} intervals. Bands marked with asterisk are due to CH_2Cl_2 (1424 cm^{-1}) or to excess ImH (1259 and 1431 cm^{-1}).

(ImH)Fe^{II} complex, however, shows an enhanced (2200 cm^{-1}) splitting. This is attributed to the enhanced polarizability of the low-spin Fe^{II} complex, due to Fe^{II} $d_\pi \rightarrow$ porphyrin π^* back-bonding, which is also evidenced by shifts in the ground-state RR frequencies (vide infra).

The splitting and/or red-shift of the B band in aqueous porphyrin solutions has long been associated with aggregation,[25] which results from hydrophobic interactions between the porphyrin rings and side chains. In the case of heme *a*, the long farnesyl side chain no doubt plays an important role in such interactions. The red shift of part of the B band is attributable to exciton splitting, as has recently been demonstrated for covalently linked porphyrins.[27] The interaction of the strong B transition dipoles produces symmetric and antisymmetric combinations, with energy separation and intensities dependent on the dipole strength, distance, and orientation. The much weaker Q transitions are not observably split. While one naturally thinks of stacking interactions between porphyrin rings in aggregates, and a stacked geometry has recently been demonstrated by NMR[28] spectroscopy for a dicyano–hemin dimer in methanol at low temperature, stacking is not a requirement for exciton splitting. B-band splitting of the magnitude observed in aqueous aggregates can be produced by lateral interactions over reasonable intermolecular distances.[27] The molecularity in aqueous porphyrin solutions is uncertain; at least at low concentration there is a time dependent intensification of the red-shifted B-band component, presumably reflecting a slowly increasing extent of aggregation.[25a] The intermolecular forces responsible for aggregation do not appear to alter the ground-state structure, since the RR frequencies are essentially the same in water, detergent, or nonaqueous solution, except for specific

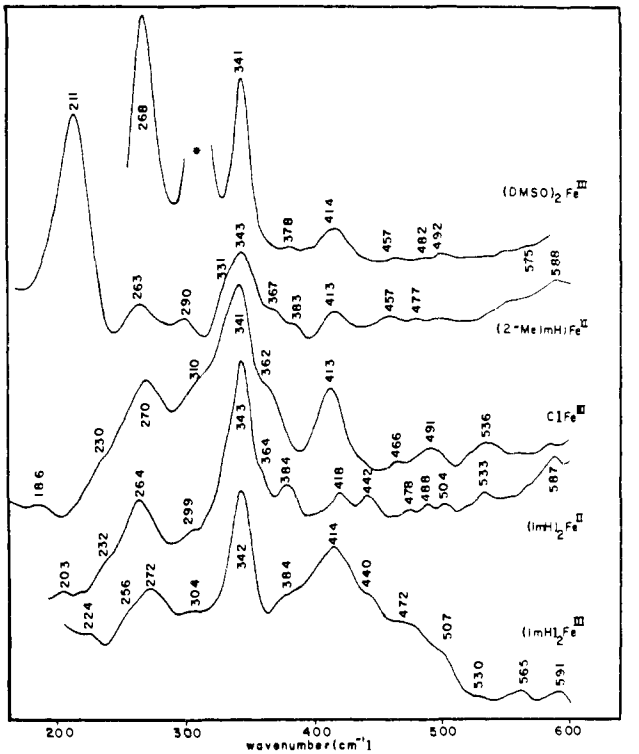

Figure 5. RR spectra, below 600 cm^{-1}, with B-band excitation for heme *a* complexes as in Figure 4, except Cl$Fe^{III}Pa$ was in 20% (v/v) $MeOH/H_2O$, λ_0 = 4067 Å; and $(ImH)_2Fe^{II}Pa$ was in Brij-35 (2%), λ_0 = 4545 Å. Band marked with asterisk is due to Me_2SO (308) cm^{-1}.

H-bond effects. There are, however, intensity changes, reflecting altered resonance conditions and scattering mechanisms[16] (vide infra).

B. Heme *a* RR Spectra. Biologically occurring porphyrins, including heme *a*, have carbon substituents at the pyrrole C_b atoms and hydrogen at the methine C_m atoms. They can all therefore be expected to share a common pattern of vibrational modes. This pattern is most easily analyzed in a porphyrin with eight identical pyrrole substituents, having full 4-fold symmetry, and the in-plane skeletal modes of NiOEP (OEP = octaethylporphyrin) have been assigned by Kitagawa et al.,[29] using IR and variable-wavelength RR spectroscopy, including analysis of combination modes, and supported with a normal coordinate analysis.[30] We were subsequently able to assign the analogous modes of NiPP (PP = protoporphyrin) and to identify modes of the vinyl substituents.[14] These assignments were then used to correlate the RR spectra of representative protoheme complexes.[15] In the low-frequency region out-of-plane porphyrin modes were also identified.[16] The same approach was adopted in the present study, with protoheme complexes providing reference spectra for the analysis of heme *a* modes. Tables I and II show this comparison and give the resulting assignments in the regions 1000–1700 cm^{-1} and 180–1000 cm^{-1}, for a series of standard complexes chosen to represent the oxidation, spin, and ligation states commonly found in heme proteins, namely six-coordinate, low-spin Fe^{II} or Fe^{III} (bis(ImH) complexes), five-coordinate, high-spin Fe^{II} or Fe^{III} (2-MeImH and chloride complexes), and six-coordinate, high-spin Fe^{III} (bis-(Me_2SO) complex). Figures 4 and 5 show survey heme *a* RR spectra, with B-band excitation, in the high- and low-frequency regions.

The spectra were obtained for samples dissolved in nonaqueous solvents and in water, with and without added detergent (Brij-35). Aqueous solutions introduce the complication of aggregate formation, as discussed in the preceding section, but also provide additional possibilities for resonance enhancement via the shifted and split absorption bands. Figure 6 shows spectra of

(27) Selensky, R.; Holten, D.; Windsor, M. W.; Paine, J. B., III; Dolphin, D.; Gouterman, M.; Thomas, J. C. *Chem. Phys.* **1981**, *60*, 33–46.
(28) LaMar, G. N.; Viscio, D. B. *J. Am. Chem. Soc.* **1974**, *96*, 7354–7355.
(29) Kitagawa, T.; Abe, M.; Ogoshi, H. *J. Chem. Phys.* **1968**, *69*, 4516.
(30) Abe, M.; Kitagawa, T.; Kyogoku, Y. *J. Chem. Phys.* **1978**, *69*, 4526.

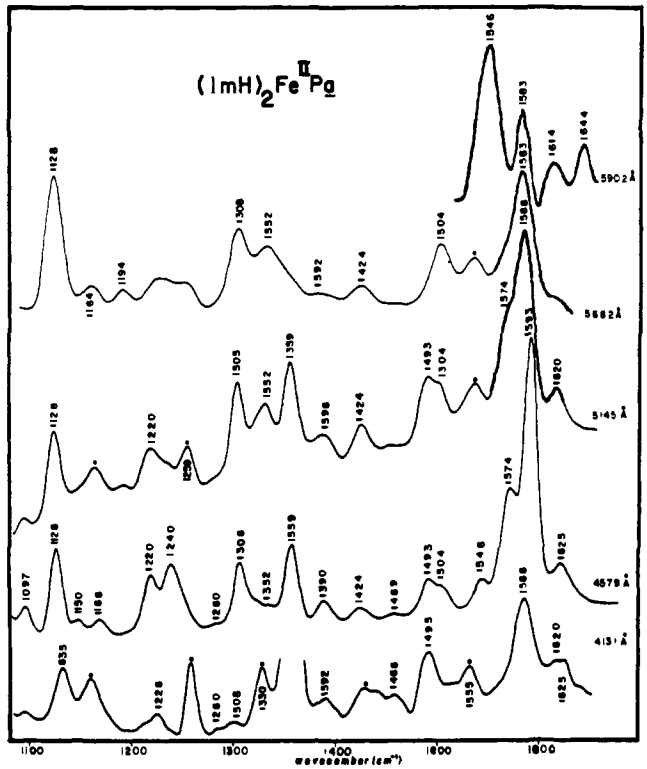

Figure 6. RR spectra of $(ImH)_2Fe^{II}Pa$ in H_2O at wavelengths (4131, 4579, 5145, 5902 (in Me_2SO) Å) in resonance with different absorption bands (Figure 2). Conditions as in Figure 4. Bands marked with asterisk (1164, 1259, 1330, 1431, 1535 cm^{-1}) are due to excess ImH.

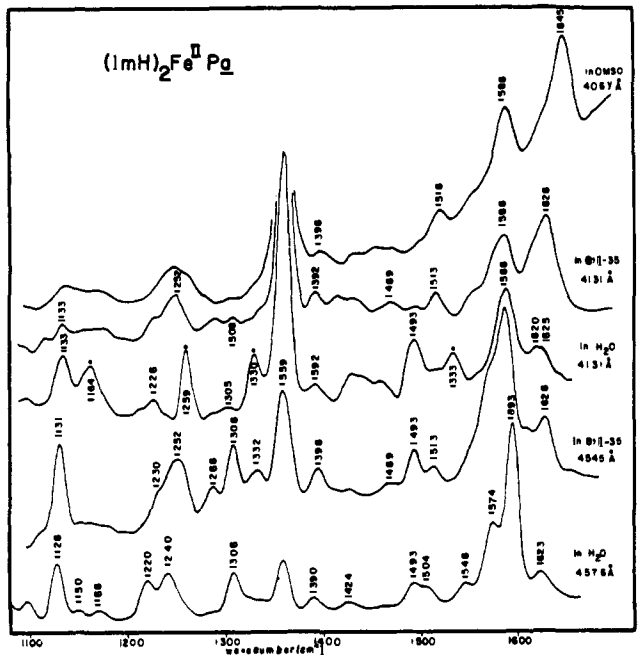

Figure 7. RR spectra above 1000 cm^{-1} of $(ImH)_2Fe^{II}Pa$ in Me_2SO (λ_0 = 4067 Å), in Brij-35 (λ_0 = 4131, 4545 Å) and in H_2O (λ_0 = 4131, 4579 Å) conditions as in Figure 4. Bands marked with asterisk are due to excess ImH.

$(ImH)_2Fe^{II}Pa$ with five different excitation wavelengths, in resonance (see Figure 2) with the absorptions assigned to Q_{y0}, Q_{y1}, Q_{x1}, and both excitonic components of the B transition. The differing patterns of selective enhancement are very useful in assigning the vibrational modes (vide infra). Aqueous solutions also provide for H bonding of the heme *a* formyl group, which is an important determinant of the spectra. Addition of detergent disperses the aqueous aggregates, and diminishes (but does not eliminate; vide infra) formyl H bonding. Figure 7 compares

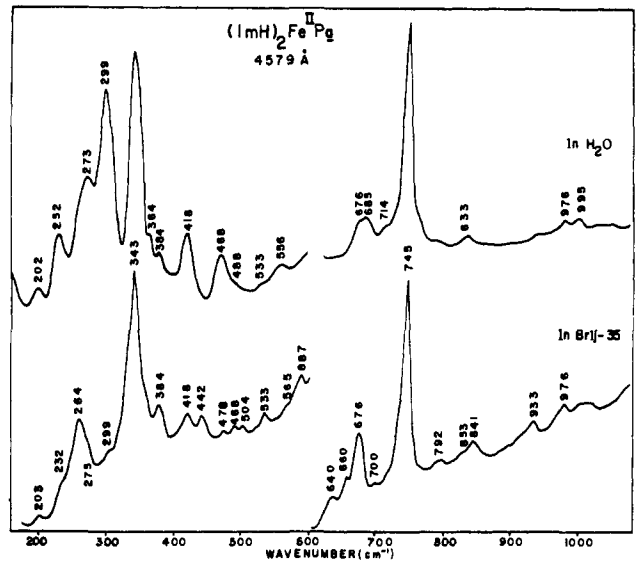

Figure 8. RR spectra below 1000 cm^{-1} of $(ImH)_2Fe^{II}Pa$ in H_2O and in Brij-35, λ_0 = 4579 Å. Conditions as in Figure 4.

aqueous $(ImH)_2Fe^{II}Pa$ RR spectra with and without Brij-35, using B-band excitation. The marked changes observed upon detergent addition can all be explained by changes in the enhancement pattern and by diminished formyl H bonding. There is no evidence for vibrational frequency shifts associated with aggregation per se. This is not surprising, since the aggregates are held together by weak hydrophobic forces, which are unlikely to alter the ground-state porphyrin structure appreciably. This is also the case in the low-frequency region (Figure 8), where some remarkable intensity differences are observed.

C. Vinyl Modes. Nearly all of the vibrational modes of the vinyl group have been identified in RR and IR spectra of protoporphyrin complexes via their frequency shifts upon deuteration of the vinyl C_α or C_β atoms.[14,15] Their RR enhancements are attributable to electronic interaction of the vinyl and porphyrin π systems in the excited state and to vibrational coupling of vinyl and porphyrin modes in the ground state. A direct indication of vibrational coupling was the observation of separate bands for the in- and out-of-phase combinations of the local modes of the two vinyl groups (Figure 1), with frequency separations of up to ~100 cm^{-1}.[14] The vinyl mode frequencies were found to be largely independent of the nature of the protoporphyrin complex.[15]

Vinyl modes are also expected to appear in heme *a* RR spectra, but there should only be one of each kind, since there is only one vinyl group, at position 4 (Figure 1). Since vinyl-deuterated heme *a* was unavailable, we tentatively assigned the vinyl modes by using correlations with protoheme spectra, as indicated in Tables I and II. A ~1620-cm^{-1} band is always seen in B-excited heme *a* RR spectra and is assignable to $\nu_{C=C}$, as in protoheme spectra. Two vinyl CH_2 scissors modes are observed for protoheme, at ~1430 and ~1340 cm^{-1}; for the heme *a* complexes the ~1430-cm^{-1} region is blank, but a band is seen at ~1335 cm^{-1}, with both B and Q excitation (although its polarization, anomalous in protoheme, is uninformative for heme *a*; vide infra) and is assigned to $\delta_{s=CH_2}$. The $C_\alpha H$ in-plane bend, $\delta_{CH=}$, is seen at ~1305 cm^{-1} upon B excitation of protoheme, and a similar band is seen for heme *a*. The out-of-plane bend, $\gamma_{CH=}$, seen at 1008 cm^{-1} for protoheme, is tentatively identified only in the (2-MeImH)$Fe^{II}Pa$ spectrum. The porphyrin–vinyl stretch, $\nu_{C_b-C_\alpha}$ has been identified at ~1170 cm^{-1} in protoheme RR spectra; a similar band is seen for heme *a* complexes. Finally, heme *a* complexes show a band (Table II) at ~415 cm^{-1}, at one of the two frequencies where bending modes of the vinyl group, $\delta_{C_bC_\alpha C_\beta}$, have been identified for protoheme.

D. Formyl Modes. Formyl modes are also expected in heme *a* RR spectra, and indeed a band at 1676 cm^{-1}, well above all the porphyrin skeletal modes, was assigned to formyl C=O stretching in the early cytochrome oxidase spectrum reported by Salmeen

Table I. RR Frequencies (cm^{-1}) of Heme *a* and Protoheme Complexes above 1000 cm^{-1}

assignment[a]			$(ImH)_2Fe^{III}$			$(ImH)_2Fe^{II}$			$ClFe^{III}$			$(Me_2SO)_2Fe^{III}$			(2-MeImH)Fe^{II}		
			Pa[b]	PP	Δ[c]	Pa	PP[b]	Δ	Pa	PP	Δ	Pa	PP	Δ	Pa	PP	Δ
		ν_{CO}	1666			1644			1671			1666			1660		
		$\nu_{CO\cdots H}$	1656			1628[d]			1656						1645		
ν_{10}	B_{1g}	C_aC_m	1640	1640	0	1620	1617	3	1632	1626	6	1609	1610	−1	1607	1604	3
		$\nu_{C=C}$	1624	1620	4	1623	1620	3	1629	1626	3	1620	1621	−1	1624	1622	2
ν_{37}	E_u	C_bC_b		1602		1614 1588	1604	10 −16		1591		1558	1580	−22	1563	1583	−20
ν_{19}	A_{2g}	C_aC_m	1589	1586	3	1583	1583	0		1571			1560			1550	
ν_2	A_{1g}	C_bC_b	1588	1579	9	1593	1584	9	1577	1570	7	1567	1559	8	1578	1562	16
ν_{11}	B_{1g}	C_bC_b	1553[e]	1562	−9	1504[f]	1539	−35		1553		1520	1545	−25		1547	
			1562	1554	8	1574	1560	14	1540	1533	7		1518		1533	1521	12
			1540		−14	1546		−14	1520		−13				1496		−25
ν_3	A_{1g}	C_aC_m	1503	1502	1	1493	1493	0	1491	1491	0	1478	1480	−2	1472	1471	1
ν_{28}	B_{2g}	C_aC_m	1473	1469	4	1469	1461	8	1470	1453	17	1444	1447	−3	1443		
		$\delta_{s=CH_2(1)}$		1435			1431			1435						1426	
$\nu_{20,29}$	A_{2g}, B_{2g}		1402	1399	3	1392	1392	0	1395			1394			1397		
		δ_{C-H}	1390			1390									1392		
ν_4	A_{1g}	C_aN	1375	1373	2	1359	1359	0	1372	1373	−1	1369	1370	−1	1356	1357	−1
		$\delta_{s=CH_2(2)}$	1331	1346	−15	1332	1337	−5	1339	1340	−1	1335			1330	1338	−8
ν_{21}	A_{2g}	δ_{C_mH}		1306		1305	1306	−1	1310	1309	−1	1314	1313	−1		1302	
		$\delta_{CH=}$	1314	1305	9	1308	1306	3		1308			1311		1311	1305	6
ν_{42}	E_u	δ_{C_mH}	1284			1280			1267			1284			1287	1285	2
$\nu_5+\nu_9$			1248	1260	−12	1240	1254	−14	1256	1260	−4	1248	1239	9	1247		
ν_{13}	B_{1g}	δ_{C_mH}		1230		1226	1225	1		1228			1225			1227	
		ν_{C_b-CHO}	1239			1220[g]			1231			1228			1232		
ν_{30}	B_{2g}	C_b-S	1173	1167	6	1168	1174	−6	1173	1170	3	1174	1170	4	1174	1170	4
$\nu_6+\nu_8$			1133	1130	3	1133	1130	3	1130	1130	0	1136	1130	6	1138	1130	8
ν_{22}	A_{2g}	C_aN		1125		1128	1125	3		1125		1124	1127	−3	1119	1122	−3
		$\delta_{as=CH_2}$				1084	1089	−5		1089			1089			1087	
ν_{45}	E_u	CaN		997		995	995									999	
		$\gamma_{CH=}$		1008			1008			1008			1008		1007	1005	−2

[a] Skeletal mode numbers, and (D_{4h}) symmetries, with major potential energy contributor as calculated for NiOEP by Abe et al.;[30] vinyl and formyl assignments as described in the text. [b] Pa = porphyrin *a*; PP = protoporphyrin IX. [c] Frequency difference between Pa and PP complexes. [d] Frequency in Brij-35; in water it shifts down further, to ~1623 cm^{-1}. [e] Observed with 5682 Å excitation (not shown). [f] Frequency of 1504 cm^{-1} in H_2O, but 1513 cm^{-1} in Brij-35 and 1518 cm^{-1} in Me_2SO. [g] Frequency of 1220 cm^{-1} in H_2O, but 1229 cm^{-1} in Brij-35, and ~1240 cm^{-1} in Me_2SO.

et al.[2] This band has drawn a good deal of attention since then. Babcock and co-workers[11] established that the 1660-cm^{-1} band of (2-MeImH)Fe^{II}P*a* in CH_2Cl_2 is lowered by ~20 cm^{-1} in water and attributed this shift to H bonding of the formyl group. They also assigned a 1644-cm^{-1} band of (*N*-MeIm)$_2Fe^{II}$P*a* in CH_2Cl_2, shifting down further in H_2O, to $\nu_{C=O}$.

Our spectra confirm these observations and extend them to the Fe^{III} complexes. The formyl C=O frequencies in water($\nu_{CO\cdots H}$) and nonaqueous solvents (ν_{CO}) are listed in Table I. In every case, the downshift on H_2O H bonding is 10–20 cm^{-1}. The $\nu_{CO\cdots H}$ position in aqueous $(ImH)_2Fe^{II}$P*a* is difficult to determine because of overlap with the vinyl $\nu_{C=C}$, and skeletal mode ν_{10}, both of which are expected at 1620 cm^{-1}. However, an additional band can be discerned at ~1623 cm^{-1} in water and at 1628 cm^{-1} in aqueous detergent. Thus the H bond lowering appears to be 20 cm^{-1} in water and 15 cm^{-1} in detergent. In the detergent micelles the formyl group may be accessible to H_2O, although the strength of the H bond is diminished.

Relative to the 1666-cm^{-1} $\nu_{C=O}$ frequency of both the high- and low-spin six-coordinate Fe^{III} complexes, $(ImH)_2Fe^{III}$P*a* and $(Me_2SO)_2Fe^{III}$P*a*, the five-coordinate $ClFe^{III}$P*a* $\nu_{C=O}$ is 5 cm^{-1} higher, while the five-coordinate (2-MeImH)Fe^{II}P*a* $\nu_{C=O}$ is 6 cm^{-1} lower. For $(ImH)_2Fe^{II}$P*a*, $\nu_{C=O}$ is much lower (22 cm^{-1}), and we attribute this to the specific effect of d_π porphyrin π^* back-bonding in low-spin Fe^{II} hemes.[15,31] This delocalization apparently includes the formyl π^* orbital to a significant extent, resulting in a lowered $\nu_{C=O}$; the vinyl group, however, does not appear to be involved in the (ground state) delocalization since its $\nu_{C=C}$ is unaltered.

In addition to $\nu_{C=O}$ there are other local modes of the formyl group, including CH in- and out-of-plane bending (the high-frequency C–H stretch is not expected to influence the RR spectra), CO in- and out-of-plane bending, and ring–formyl stretching and bending. These have been assigned in simple aldehydes, and specific isotope shifts upon formyl deuteration are observed. The frequencies and -CDO shifts for benzaldehyde,[32,33] which should be a good model, are listed in Table III. Some of these modes can be expected to appear in heme *a* RR spectra, by analogy with the vinyl modes, and we endeavoured to locate them by preparing $(ImH)_2Fe^{II}$P*a* in an alkaline KCN solution in D_2O, a procedure that is expected[21] to lead to rapid exchange of the -CHO proton. The resulting RR spectra are compared to those obtained in H_2O in Figures 9 and 10. (It might have been expected that CN^- would replace ImH in the complex, but this was apparently prevented by the presence of excess imidazole in the solution, as evidenced by the persistence of the 202-cm^{-1} band (Figure 10) which has been assigned[34,35] to Fe–$(ImH)_2$ stretching. In any event the replacement of one strong field axial ligand for another would not have affected the formyl frequencies.)

The ring–formyl stretch, ν_{C_b-CO}, is clearly identified at 1220 cm^{-1} by its 10-cm^{-1} D/H upshift, also seen in benzaldehyde (1206 → 1217 cm^{-1}). The upshift results from coupling with th δ_{H-CO} in-plane bend, at 1390 cm^{-1}, which shifts across the ring–formyl stretch upon deuteration. The 1390-cm^{-1} band of $(ImH)_2Fe^{II}$P*a* contains contributions from two skeletal modes, ν_{20} and ν_{29}, but its 2-cm^{-1} upshift upon formyl deuteration suggests a δ_{H-CO} contribution as well. A new band appears at 1077 cm^{-1} and is assigned to δ_{D-CO} (1043 cm^{-1} in benzaldehyde). The in-plane CO

(31) Spiro, T. G.; Burke, J. M. *J. Am. Chem. Soc.* **1976**, *98*, 5482.

(32) Zwarich, R.; Smolarek, J.; Goodman, L. *J. Mol. Spectrosc.* **1971**, *38*, 336–357.

(33) Green, J. H. S.; Harrison, D. J. *Spectrochim. Acta, Part A* **1976**, *32A*, 1265–1277.

(34) Desbois, A.; Lutz, M. *Biochim. Biophys. Acta* **1981**, *671*, 168–176.

(35) Mitchell, M.; Choi, S.; Spiro, T. G., submitted for publication.

Table II. RR Frequencies (cm^{-1}) of Heme *a* and Protoheme Complexes below 1000 cm^{-1}

assignment[a]			$(ImH)_2Fe^{III}$		$(ImH)_2Fe^{II}$			$ClFe^{III}$		$(Me_2SO)_2Fe^{III}$		(2-MeImH)Fe^{II}	
					Pa		PP in					Pa in	PP in
			Pa[b]	PP[b]	Brij	H_2O	H_2O	Pa[c]	PP[c]	Pa[d]	PP[d]	Brij	TX-100
ν_{45}	E_u	C_aN		997		995	995						999
ν_{32+35}				973	976	976	976					979	982
ν_{46}	E_u	C_bS		952	933		925					930	921
		γC_mH		845	841		841			847		846	
					833	833				824			
ν_6	A_{1g}	$\delta C_aC_mC_a$		804		819			806	806		819	
ν_{32}	B_{2g}	δC_bS	798	791	792		791				786	792	788
ν_{16}	B_{1g}	δC_aNC_a	750	749	745	745	748		756	761	760	755	752
ν_{47}	E_u	C_bS		712	700	714	717		722	720		717	714
						685							
ν_7	A_{1g}	δC_bC_aN	682	677	676	676	675		675	680	677	682	676
					660							658	
		δCO			640							642	
ν_{48}	E_u	δC_bS	591	605	587	588		586		575		588	585
ν_{47}	E_u	$\delta C_aC_bC_b$	565	561	565	556	558		555				548
		pyr fold	530		533	533		536		530			
		pyr fold		510	504		507						510
		pyr fold			488		488	491	492	492	495	497	495
		pyr fold	472		478	468		466		482		477	
		pyr fold	440		442					457		457	
		pyr fold		425		426			425				
		$\delta C_bC_\alpha C_\beta(1)$	414	419	418	418	412	413	415	414	414	413	410
		γC_bS			384	384	384		380			383	374
$2\nu_{35}$			384	380	364			362	373	378	375	367	
ν_8	A_{1g}	δC_bS	342	349	343	343	345	341	345	341	344	343	345
		$\delta C_bC_\alpha C_\beta(2)$		312			312						326
		γC_aC_m	304	296	299	299	298	310	312			290	303
ν_9	A_{1g}	δC_bS	272	276	273	273	263	270	266	268	270		
		pyr tilt	256		264		254					263	255
			224	236	232	232	237	230					
ν_L[e]				200	203	202	201					211	204

[a] Assignments as in ref 16 for PP complexes. [b] In H_2O. [c] In MeOH. [d] In Me_2SO_4. [e] Fe-ligand (ImH or 2-MeImH) stretch.

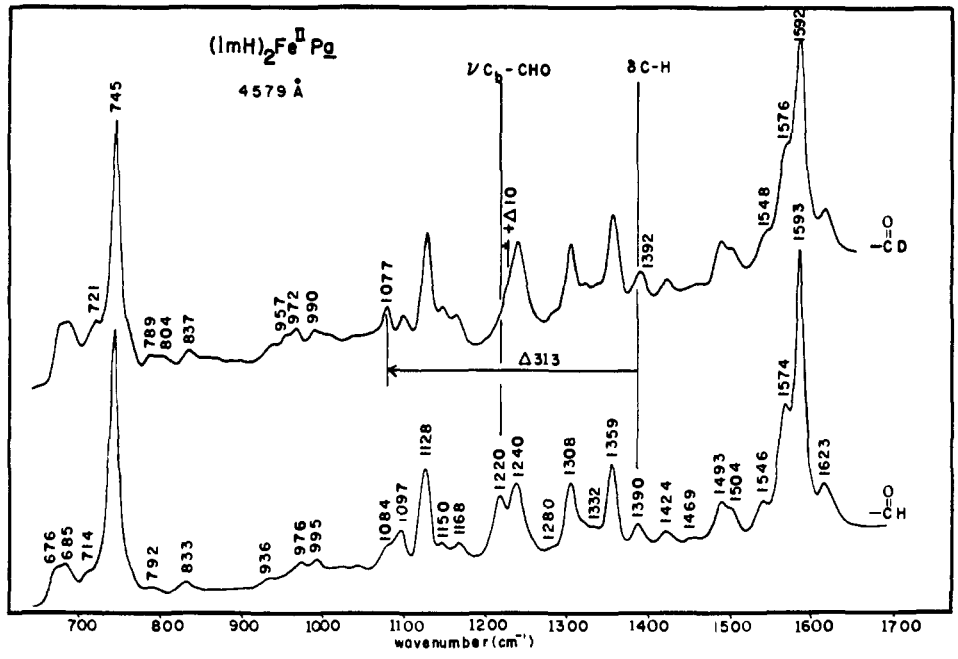

Figure 9. RR spectra above 600 cm^{-1} of $(ImH)_2Fe^{II}Pa$ in KCN/H_2O and KCN/D_2O; pH (pD) 11. (heme *a*) = 50 μM, (ImH) = 0.1 M, (CN^-) = 0.3 mM. λ_0 = 4579 Å. Conditions as in Figure 4.

bend is found at 649 cm^{-1} in benzaldehyde, shifting down 8 cm^{-1} upon -CHO deuteration. No band is seen at this frequency for aqueous $(ImH)_2Fe^{II}Pa$, but a weak band does appear at 640 cm^{-1} upon detergent addition (Figure 8) and might be δ_{CO}. Unfortunately detergent could not be added to the $KCN-D_2O$ solution without precipitate formation. The remaining formyl modes seen in benzaldehyde are the in- and out-of-plane ring–formyl bends, at 229 and 245 cm^{-1} shifting down by 7 and 25 cm^{-1} on deuteration. While $(ImH)_2Fe^{II}Pa$ bands are seen in this region (Figure 10) they do not shift down on deuteration. Slight D_2O upshifts are seen for several of the low-frequency modes, and the band at 488 cm^{-1} shifts down by 6 cm^{-1}. This band is assigned to an out-of-plane pyrrole folding mode (vide infra) and its downshift is reminiscent of that observed (Table III) for a 449-

Table III. Formyl-Related Frequencies (cm^{-1}) of Benzaldehyde (CHO/CDO) and $(ImH)_2$Heme a^{2+} (CHO/CDO)

	benzaldehyde[a]			$(ImH)_2$heme a^{2+}			
assignment[a]	CHO	CDO	Δ[b]	CHO	CDO	Δ	assignment[c]
ν_{CO}	1694	1689	−5	1593	1592	−1	ν_2 A_{1g}
				1574	1576	2	ν_{38} E_u
				1546	1548	2	ν_{38} E_u
				1504	1505	1	ν_{11} B_{1g}
$\delta_{H\text{-}CO}$	1389	1043	−346	1390	1077	−313	$\delta_{H\text{-}CO}$
$\nu_{Ph\text{-}CHO}$	1206	1217	11	1220	1230	10	$\nu_{C_b\text{-}CHO}$
$\gamma_{H\text{-}CO}$	1009[d]	863	−137				
	825	792	−23				
δ_{CO}	649	641	−8	488	482	−6	pyr fold
				468	472	4	pyr fold
ring bending twist	449	446	−3				
				364	368	4	γ_{C_bS}
				343	345	2	ν_8 A_{1g}
				299	301	2	$\gamma_{C_aC_m}$
$\gamma_{Ph\text{-}CHO}$	245	220	−25				
$\delta_{Ph\text{-}CHO}$	229	222	−7				

[a] Assignment of benzaldehyde modes from ref 32. [b] Frequency shift upon formyl deuteration. [c] Assignments of porphyrin modes follow Tables I and II. [d] IR frequency.

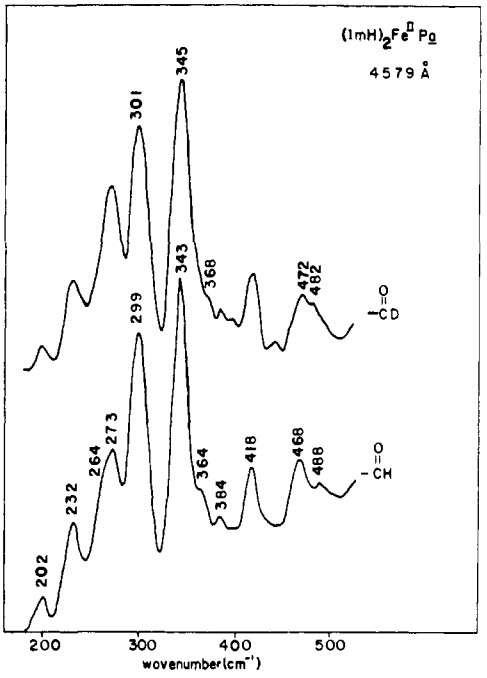

Figure 10. RR spectra below 600 cm^{-1} of $(ImH)_2Fe^{II}Pa$, as in Figure 9.

cm^{-1} ring bending twist mode of benzaldehyde.

The 1220-cm^{-1} ring–formyl stretch appears to be sensitive to H bonding, since it shifts up to 1230 cm^{-1} in detergent (see bottom two spectra in Figure 7) and up even further (obscured by an overlapping band) in Me_2SO (top spectrum in Figure 7). The direction of the shift is the same as that observed for $\nu_{C=O}$, and the magnitude is similar. It is reasonable that the two vibrations should be coupled.

The $\nu_{C=O}$ band of benzaldehyde also shifts down by ~5 cm^{-1} upon deuteration. A similar effect can be seen for $(ImH)_2Fe^{III}Pa$ in Figure 11. In H_2O $\nu_{C=O}$ appears as a 1656-cm^{-1} shoulder on the 1640-cm^{-1} ν_{10} band, and it clearly shifts under the ν_{10} envelope upon KCN–D_2O treatment.

E. Porphyrin Skeletal Modes. Comparison of NiOEP and NiPP RR spectra showed three distinct effects of the vinyl substituents: (a) enhancement of vinyl modes, as discussed above, (b) activation of (IR-active) E_u skeletal modes due to the loss of the electronic symmetry center, induced by the asymmetrically disposed vinyl substituents, and (c) vibrational coupling between vinyl and skeletal modes, producing pairs of vinyl modes, and some frequency shifts of the skeletal modes. These effects are all seen

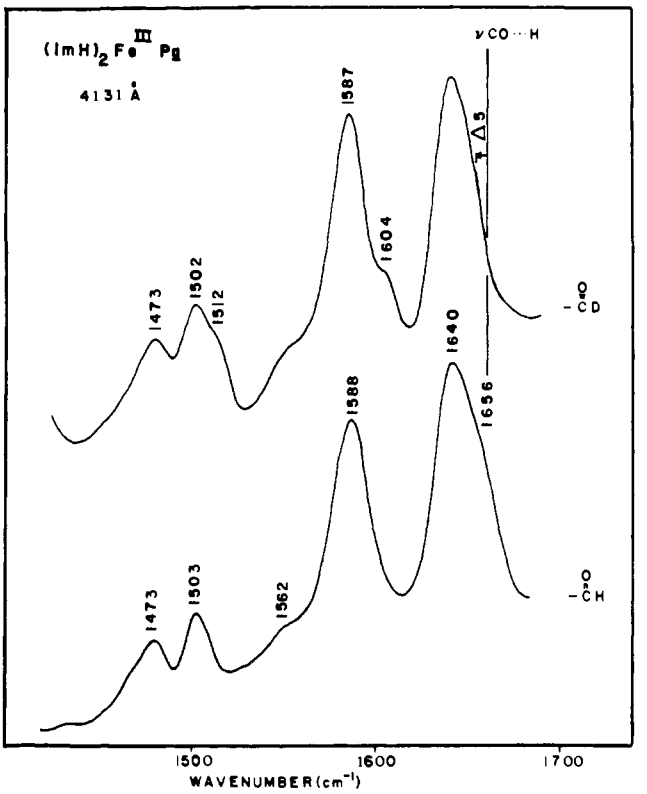

Figure 11. RR spectra of $[(ImH)_2Fe^{III}Pa]^+$ in KCN/H_2O and KCN/D_2O, pH (pD) = 11. Concentrations as in Figure 9. λ_0 = 4131 Å. Conditions as in Figure 4, except slit width = 5 cm^{-1}.

in heme *a* as well, but the *x,y* electronic splitting produced by the trans disposition of the formyl and vinyl groups has additional consequences: (1) The depolarization ratios tend toward $^1/_3$, the value expected[36] when the Raman tensor is dominated by a single diagonal element, e.g., α_{xx} or α_{yy}. (2) E_u modes are not only activated, but also split, by up to 35 cm^{-1}, and show selective enhancement via the *x*- and *y*-polarized electronic transitions. (3) There are additional skeletal mode frequency shifts associated with the C=O delocalization. The last two effects imply some distortion of the heme *a* ground state.

1. Depolarization Ratios. Table IV lists depolarization ratios, ρ, measured for $(ImH)_2Fe^{II}Pa$, $[(ImH)_2Fe^{III}Pa]^+$ and (2-MeImH)$Fe^{II}Pa$. As was also observed by Babcock et al.,[23] most

(36) Spiro, T. G.; Stein, P. *Annu. Rev. Phys. Chem.* **1977**, *28*, 501.

Table IV. Raman Band Depolarization Ratios[a]

	(ImH)$_2$heme a^{3+}					(ImH)$_2$heme a^{2+}						(2-MeImH)heme a^{2+}		
	cm^{-1}	4131[b]	4067[c]	5145	5682	cm^{-1}	4131[b]	4579	5145	5682	5902[f]	cm^{-1}	4067[b]	4579
ν_{CO}	1656	p[d]	0.28	e		1628	p				p	1645	p	0.33
ν_{10}	1640	p	0.35	0.47	0.43	1620	p		0.54	0.44		1607	p	0.35
$\nu_{C=C}$	1624	p				1623	p	0.31				1624	p	0.39
ν_{37y}						1614					p			
ν_{37x}						1588	p		0.68			1563	p	0.40
ν_{19}	1589			0.67	0.90	1583				0.42	0.81			
ν_2	1588	p	0.40			1593		0.35				1578	p	0.36
ν_{11}	1533				0.60	1504		0.36	0.36	0.40	p			
ν_{38x}	1562	p		0.53		1574		0.33	0.64			1533	p	0.58
ν_{38y}	1540			0.40		1546		0.33			p	1496		0.33
ν_3	1503	p	0.20	0.40		1493	p	0.33	0.29			1472	p	0.35
ν_{28}	1473		0.51			1469	p	p				1443		0.31
ν_{20}	1402	p		0.57	0.50	1396			0.83					
ν_{29}						1392	p			p		1397		0.53
δ_{CH_2}						1390		0.36			p	1392	p	
ν_4	1375	p	0.33	0.43		1359	p	0.28	0.45			1356	p	0.36
$\delta_{s=CH_2}$	1331	p		0.31		1332		0.39	0.42	0.40	p	1330		0.73
ν_{21}	1310	p		0.68	0.80	1305	p		0.50			1311	p	0.68
$\delta_{CH=}$						1308		0.38		0.40	p			
ν_{C_bCHO}	1239	p	0.48			1220		0.35	0.20		p	1226	p	p
ν_{30}	1173	p		0.47		1168	p	0.33			p	1174	p	
$\nu_6 + \nu_8$	1133	p	0.60	0.42		1133	p					1138	p	
ν_{22}						1128		0.36	0.43	p	p			

[a] $I_\perp/I_\parallel$; the samples were in aqueous solution. [b] Excitation wavelength (Å). [c] Data from ref 9. [d] Bands marked p were observed to be polarized, but the intensities were inadequate for depolarization ratio determination. [e] Not observed. [f] For this spectrum, the sample was in Me_2SO.

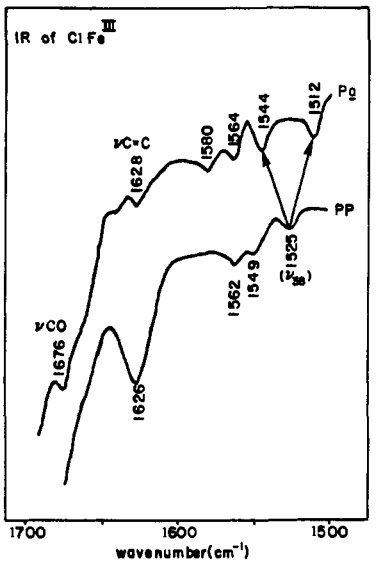

Figure 12. FTIR spectra of ClFe^{III}PP and ClFe^{III}P*a* in CsI pellet. Conditions: resolution, 8 cm^{-1}; sensitivity, 1.

Table V. IR Frequencies of ClFe^{III}PP and ClFe^{III}P*a* in CsI

E_u modes		PP	P*a*	Δ[a]	substituent modes
		1735	1740	5	
		1705	1708	3	ν_{COOH}
			1676		ν_{CO}
		1626	1628	2	$\nu_{C=C}$
	C_bC_b		1580		
			1544	19	
ν_{38}	C_aC_m	1525	1512	−13	
ν_{39}	C_aC_m	1458	1462	4	
ν_{40}	C_aC_b	1441	1439	−2	
ν_{41}	C_aN	1381	1378	−3	
		1338	1338	0	$\delta_{s=CH_2}(2)$
		1301	1301	0	$\delta_{CH=}$
ν_{42}	δC_mH	1280	1260	−20	
ν_{43}	C_bS	1150	1140	−10	
ν_{44}	C_bS	1122	1116	−6	
		1087			$\delta_{as=CH_2}$
		1004			$\gamma_{CH=}$
ν_{45}	C_aN	988	998	10	
ν_{46}	C_bS	920	917	−3	$\gamma_{s=CH_2}$
	γC_mH	848	838	−10	
ν_{47}	C_bS	712	721	9	
			639		δ_{CO}

[a] Frequency difference between P*a* and PP.

of the values are not far from $^1/_3$, whether the bands correlate with A_{1g} (ν_2,ν_3,ν_4), B_{1g} (ν_{10},ν_{11}) or B_{2g} ($\nu_{28},\nu_{29},\nu_{30}$) modes of OEP. In D_{4h} symmetry A_{1g} modes are expected[36] to have $\rho = {}^1/_8$, since $\alpha_{xx} = \alpha_{yy}$ (and α_{zz} should be zero for resonance with an in-plane polarized (x,y) electronic transition). But if the x and y electronic levels are split, then resonance with one or the other gives a single dominant tensor element and ρ rises to $\sim{}^1/_3$. The B_{1g} tensor has $\alpha_{xx} = -\alpha_{yy}$, and $\rho = {}^3/_4$; again dominance of either α_{xx} or $-\alpha_{yy}$, due to x,y splitting, produces $\rho \sim {}^1/_3$. The B_{2g} tensor has zero diagonal elements, and $\alpha_{xy} = \alpha_{yx}$, giving $\rho = {}^3/_4$. In this case x,y splitting must induce diagonal elements since a depolarization ratio less than $^3/_4$ requires a nonzero tensor trace;[36] this implies an effective symmetry lower than D_{2h}, e.g., C_2 or σ_h, in which B_{2g} correlates with a totally symmetric representation.

Depolarization ratios as high as 0.8–0.9 are seen with 5682-Å ([(ImH)$_2$Fe^{III}P*a*]$^+$) or 5902-Å ((ImH)$_2$Fe^{II}P*a*) excitation, in resonance with the Q bands, for RR bands correlating with A_{2g} modes ($\nu_{19},\nu_{20},\nu_{21}$). This has also been observed by Babcock et al.[23] In strictly D_{4h} symmetry, $\rho = \infty$ for A_{2g} modes, which have antisymmetric tensors ($\alpha_{xy} = -\alpha_{yx}$).[36] As the symmetry is lowered, ρ decreases, due to induced symmetric off-diagonal tensor elements ($\alpha_{xy} \neq -\alpha_{yx}$) as well as diagonal elements. However the antisymmetric part is still sufficient for these heme *a* modes to produce anomalous polarization $\rho > {}^3/_4$, with Q-band excitation.

2. E_u Modes. Direct evidence for E_u mode splitting in heme *a* is given by the IR spectrum of ClFe^{III}P*a*, compared with that of ClFe^{III}PP in Figure 12 (Table V lists the IR frequencies, with assignments). The 1525-cm^{-1} band of protoheme has been correlated[14,15] with E_u mode ν_{38} of NiOEP and is activated in the RR spectrum (appearing at 1518 cm^{-1}; see Table I). In heme *a* this mode is clearly split into two components, at 1544 and 1512 cm^{-1}. Both of these components appear in the RR spectrum (see Figure 4). Likewise, for [(ImH)$_2$Fe^{III}P*a*]$^+$, (ImH)$_2$Fe^{II}P*a*, and (2-MeImH)Fe^{II}P*a*, the RR spectra show a pair of bands whose

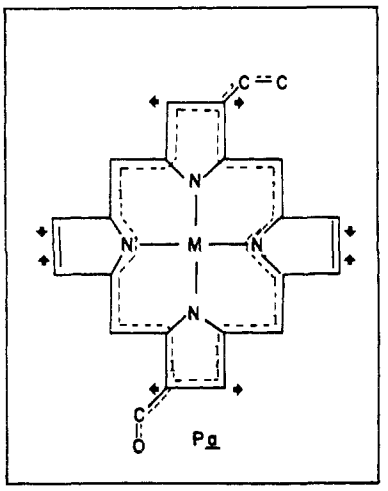

Figure 13. Eighteen-membered porphyrin π delocalization pathway (dotted line), stabilized by trans vinyl and formyl substituents of heme *a*. The arrows indicate the phasing of the B_{1g} symmetry coordinate for C_bC_b stretching, thought to account for the lowering of ν_{11} in heme *a* (see text).

frequencies flank those of the ν_{38} bands of the analogous PP complexes (see Table I); these are assigned to the split ν_{38} components. Protoheme RR spectra show a higher frequency band (1580–1605 cm^{-1}) which has been correlated with the E_u mode ν_{37} (which has low IR intensity, and escapes detection in most IR spectra). This region of the heme *a* RR spectra is difficult to resolve, but for $(ImH)_2Fe^{II}Pa$, for which the largest number of spectra have been collected, a pair of bands can be observed, at 1614 and 1588 cm^{-1}, which flank the ν_{37} frequency, 1604 cm^{-1}, of the PP analogue.

When an E_u modes is split, due to *x,y* inequivalence, one of the resulting components transforms as *x*, while the other transforms as *y*. The *x* component can be expected to show maximal enhancement in RR spectra excited at *x*-polarized electronic transitions, and likewise the *y* component should be maximally enhanced via the *y*-polarized transition. It is therefore satisfying to find that selective enhancement for one or the other component of the ν_{37} and ν_{38} modes is observed in the variable-wavelength RR spectra of $(ImH)_2Fe^{II}Pa$ (Figure 6). At 5902 Å, in resonance with the absorption band (Figure 2) identified above with Q_{y0}, one sees pronounced enhancement of the higher ν_{37} component (1614 cm^{-1}) and the lower ν_{38} component (1546 cm^{-1}), while the other pair of components (1588 cm^{-1} (ν_{37}), 1574 cm^{-1} (ν_{38})) is selectively enhanced at 5145 Å, in resonance with the absorption band identified with Q_{x0}. We therefore assign the 1614- and 1546-cm^{-1} bands to ν_{37y} and ν_{38y}, with eigenvectors producing excited-state origin shifts along the *y* (vinyl → formyl) axis, and the 1588 and 1574 cm^{-1} bands to ν_{37x} and ν_{38x}, producing *x*-directed origin shifts.

Other high-frequency E_u modes, ν_{39}–ν_{44}, are not generally seen in PP or P*a* RR spectra (although a band which appears to be ν_{42}, at ~1280 cm^{-1} is seen for the P*a* complexes, Figure 4). In the 550–1000-cm^{-1} region, weak bands have been assigned to ν_{45}–ν_{49} in PP spectra; these occur at nearly the same frequencies in P*a* spectra.

3. Skeletal Frequency Changes. Aside from the splitting of the ν_{37} and ν_{38} modes, significant frequency differences between PP and P*a* are seen for RR bands correlating with the A_{1g} mode, ν_2, which is ~10 cm^{-1} higher for P*a*, and the B_{1g} mode, ν_{11}, which is 9–35 cm^{-1} lower for P*a*. The P*a* – PP difference in ν_2 has also been noted by Callahan and Babcock.[9a] These two modes, which mainly involve stretching of the pyrrole C_b–C_b bonds, are both lower, by 10–20 cm^{-1}, in PP complexes than in the OEP analogues and are coupled to the vinyl groups, both kinematically and electronically.[14,15] We attribute the up- and downshifts in P*a*, relative to PP, to the effect of altering the porphyrin conjugation pathway via the trans disposition of the formyl and vinyl groups. As diagrammed in Figure 13, this placement of the delocalizing

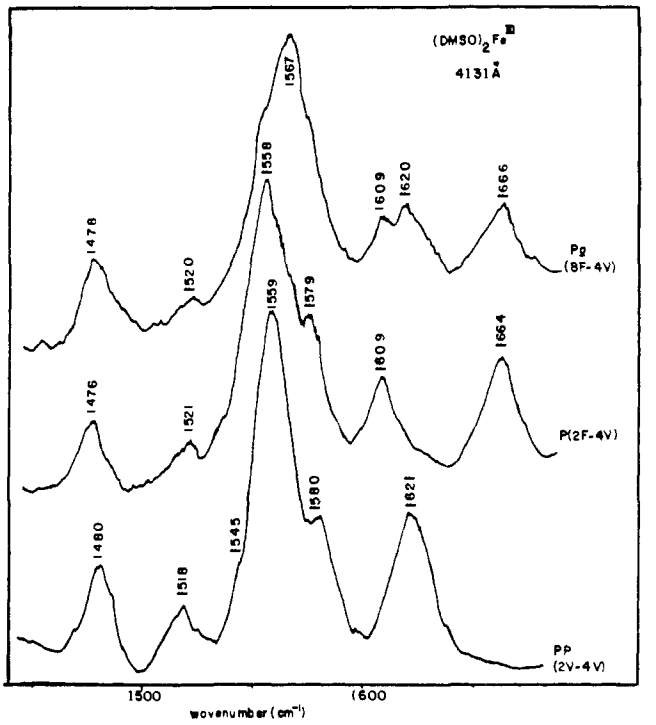

Figure 14. RR spectra (λ_0 = 4131 Å) of $(Me_2SO)_2Fe^{III}$ complexes of P*a* (8F-4V), PP (2V-4V), and of protoporphyrin with the 2-vinyl group replaced with formyl, P (2F-4V). Conditions as in Figure 4.

substituents extends and stabilizes one of the two alternative 18-membered pathways available to the porphyrin π system. Since the ν_{11} (B_{1g}) mode involves stretching of opposite pyrrole C_b–C_b bonds and contraction of adjacent ones, it is evident that the heme *a* conjugation, which should lengthen one pair of opposite C_b–C_b bonds (adjacent to the formyl and vinyl groups) and shorten the other pair, should specifically lower the ν_{11} force constant. It is less obvious why the force constant for ν_2 (A_{1g} – all C_b–C_b bands stretch and contract in phase) should increase, although alternation of frequency shifts associated with conjugation effects is not unexpected. The effect of this alternation is to place ν_2 for heme *a* in apparent coincidence with the frequency of analogues with only saturated substituents, such as OEP; ν_{11}, however, is much lower.

The important role of the trans disposition of the heme *a* substituents is demonstrated by the RR spectrum of 2-formyl, 4-vinyl heme, in which the 2-vinyl group of protoheme is replaced by a formyl group. Figure 14 compares this heme, as the bis-(Me_2SO) complex, with the analogous P*a* and PP complexes. The formyl $\nu_{C=O}$ shows up at 1664 cm^{-1}, as it does for P*a*, but the intense band arising from ν_2 is at the PP position, 9 cm^{-1} lower than P*a*. (The ν_{11} assignment is not entirely clear. A band is seen at 1520 cm^{-1} in all three spectra; this is assigned to ν_{38} for PP, but ν_{11} for P*a*, since all other P*a* complexes show a pronounced splitting of ν_{38}. ν_{11} is assigned to the 1545-cm^{-1} shoulder for PP, and is probably at the same frequency for the 2-formyl, 4-vinyl heme.) Thus the ν_2 (and probably the ν_{11}) frequency is determined by the substituent locations, and not be the presence of formyl vs. vinyl per se.

This result is consistent with observations by Tsubaki et al.[37] on myoglobin (Mb) reconstituted with either 2-formyl, 4 vinyl or 2-vinyl, 4-formyl heme. Their RR spectra, obtained with near-B-band excitation, showed a strong band, assignable to ν_2, at essentially the same frequency, for either modified heme, as observed in the native (protoheme) derivative. (The one anomaly was the 2-formyl, 4-vinyl-reconstituted deoxyMb, which shows ν_2 8 cm^{-1} lower than the native protein. The $\nu_{C=O}$ frequency was also anomalously low (1648 vs. 1665 cm^{-1} for all the other spectra),

(37) Tsubaki, M.; Nagai, K.; Kitagawa, T. *Biochemistry* **1980**, *19*, 379–385.

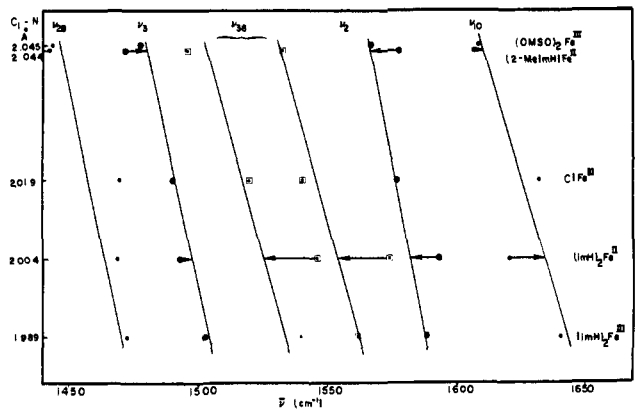

Figure 15. Skeletal mode frequencies for P*a* complexes vs. porphyrin C_t–N distance (crystallographic values for analogue porphyrin complexes, as described in ref 15). The lines are drawn with the parameters given in Table VI. Arrows indicate deviations from the lines for (2-MeImH)Fe^{II}P*a* and $(ImH)_2Fe^{II}$P*a*.

Table VI. Porphyrin Core-Size Correlation Parameters for PP and PP and P*a* Complexes

mode	slope,[a] K cm^{-1}/Å	intercept,[a] A, Å		$\Delta(ImH)_2Fe^{II}$,[b] cm^{-1}	
		PP	P*a*	PP	P*a*
ν_{10} B_{1g}	517.2	5.16	same	−17	−14
ν_{37} E_u	356.3	6.48		10	
ν_2 A_{1g}	390.8	6.03	6.05	9	11
ν_{19} A_{2g}	494.3	5.20		3	
ν_{38} E_u	551.7	4.80	4.82 (ν_{38x})	19	20
			4.77 (ν_{38y})		20
ν_{11} B_{1g}	344.8	6.53		−21	
ν_3 A_{1g}	448.3	5.35	same	−5	−5
ν_{28} B_{2g}	402.3	5.64	same	−3	5

[a] Slope and intercept for the relation $\bar{\nu} = K(A - d)$; $\bar{\nu}$ = mode wave number and d = porphyrin center-to-pyrrole nitrogen distance, C_t–N. The slopes were determined from the PP data and held fixed for P*a*. For ν_{37}, ν_{19}, and ν_{11}, P*a* assignments are incomplete. [b] Deviations for the $(ImH)_2Fe^{II}$ complexes from the frequencies expected on the basis of core size.

and it seems that a specific protein influence is expressed in this form.)

F. Core Size Correlations. The assignments listed in Table I for the complicated region above 1450 cm^{-1} are supported by the corelation of these skeletal frequencies with porphyrin core size, which have recently been documented for PP complexes.[15] Figure 15 is a plot of frequency vs. porphyrin center-to-pyrrole nitrogen (C_t–N) distance (obtained from reference porphyrin crystal structures, as described in ref 15), for those skeletal modes that could be assigned for all five complexes. The general trend of decreasing frequency with increasing core size has been attributed[38] to lowering of the ring stretching force constants principally associated with the methine bridges, whose bonds are expected to weaken as the core expands. The lines in Figure 15 are identical with those used for the analogous PP correlations, except that the ν_2 line has been shifted down by 8 cm^{-1}, without change in slope, while the ν_{38} line has been split into two branches, 11 and 17 cm^{-1} above and below the PP ν_{38} line, again without change in slope (see Table VI for slopes and intercepts). Thus once the specific effects of altered peripheral substituents are taken into account, the P*a* and PP data are seen to follow the same core size correlations.

There are three anomalous points in Figure 15, which are not understood: ν_{10} and ν_{28} for $ClFe^{III}$ and ν_2 for (2-MeImH)Fe^{II} are 6–17 cm^{-1} above the lines for P*a*, but not for PP. The lowered values of ν_3 and ν_{10} for (2-MeImH)Fe^{II} are observed for PP as well as P*a*, and have been attributed to porphyrin doming in the 5-coordinate Fe^{II} complex.[15] The large deviations of the points for $(ImH)_2Fe^{II}$ are associated with $d_\pi \rightarrow$ porphyrin π^* back-bonding in the low-spin Fe^{II} complex, and have been interpreted[15] in terms of the nodal properties of the porphyrin e_g (π^*) orbitals and the symmetries of the normal modes (in the idealized D_{4h} point group): E_u and B_{1g} modes show large positive and negative deviation from the values expected on the basis of core size, while A_{1g} modes show smaller positive and negative deviations, and B_{2g} and A_{2g} modes show minimal deviation. Table VI demonstrates that the magnitudes of the deviations are very similar for P*a* and PP. The similarity holds also for the A_{2g} mode ν_{19}, whose frequency is within 3 cm^{-1} of the core size correlation for PP. The assigned frequency is the same for P*a* as for PP. (This mode is omitted from Figure 15, since it could not be reliably assigned for P*a* complexes other than $(ImH)_2Fe^{II}$ and $(ImH)_2Fe^{III}$.)

The ν_{11} (B_{1g}) frequency (omitted from Figure 15 for the same reason) is, however, anomalously low, 1504 cm^{-1}, for $(ImH)_2Fe^{II}$P*a*, 35 cm^{-1} lower than for the PP analogue, whereas the difference is only 9 cm^{-1} for the $(ImH)_2Fe^{III}$ complex. As noted above, this C_b–C_b stretching mode is specifically lowered in frequency by the trans disposition of the P*a* formyl and vinyl groups, since its phasing assists the stabilization of the 18-membered π delocalization pathway (Figure 13). This effect appears to be amplified in the $(ImH)_2Fe^{II}$ complex, suggesting that the d_π back-bonding further stabilizes the 18-membered pathway. This extra stabilization is consistent with the enhanced x,y splitting suggested by the absorption spectrum of this complex (see above) and also with its lowered formyl C=O stretching frequency (1623 cm^{-1} in water, and 1644 cm^{-1} in nonaqueous solvents, vs. ~1650 and ~1665 cm^{-1} for the other complexes). Moreover, while ν_{11} of $[(ImH)_2Fe^{III}Pa]^+$ is at the same frequency, 1553 cm^{-1} in water or in nonaqueous solvents, it is sensitive to C=O H bonding in $(ImH)_2Fe^{II}$P*a*, shifting from 1504 cm^{-1} in water to 1511 cm^{-1} in aqueous detergent and 1518 cm^{-1} in Me_2SO, paralleling the shift of the C=O stretching frequency itself. Thus, in the $(ImH)_2Fe^{II}$ complex, H bonding appears to increase the extent of d_π back-bonding into the 18-membered π system.

G. Out-of-Plane Modes. A number of porphyrin out-of-plane deformation modes have recently been assigned in PP and OEP complexes,[16] on the basis of ^{54}Fe and of methine and vinyl deuteration frequency shifts. We assign the heme *a* modes via the spectral correspondences with the PP analogues, as listed in Table II.

Two ^{54}Fe-sensitive RR bands have been observed for $[(ImH)_2Fe^{III}OEP]^+$ at 255 and 359 cm^{-1} and assigned to coupled pyrrole tilting and substituent out-of-plane bending (γ_{C_bS}) modes.[16] Activation via nonbonded interactions of the imidazole H and pyrrole N atoms was suggested, since the bands disappeared when ImH was replaced by CN^- at the axial coordination sites. A weaker band at 320 cm^{-1} shifted down by 10 cm^{-1} on methine deuteration and was assigned to methine out-of-plane deformation, $\gamma_{C_aC_m}$. These three bands were observed for $(ImH)_2Fe^{II}$PP, at 254, 384, and 299 cm^{-1}, and for the detergent solution of $(ImH)_2Fe^{III}$P*a*, they can be seen (Figure 8) at 264, 384, and 299 cm^{-1}. It is striking that in the absence of detergent (Figure 8) the 299-cm^{-1} $\gamma_{C_aC_m}$ band is strongly intensified while the 264-cm^{-1} pyrrole tilting and 384-cm^{-1} γ_{C_bS} modes are greatly diminished. The loss in 264-cm^{-1} intensity reveals the two flanking bands, 232 and 273 cm^{-1}, which are also seen in PP and OEP complexes and are assigned to in-plane skeletal modes. This dramatic intensity reversal of the 264- and 384-cm^{-1} bands on the one hand and the 299-cm^{-1} band on the other is plausibly related to aggregate formation in the absence of detergent. Apparently the methine deformation mode (299 cm^{-1}) is involved in the excited-state distortion of the aggregate, while the role of pyrrole tilting is suppressed. These effects may reflect a specific structural role of the farnesyl side chain in the aggregate, perhaps via interaction with the methine regions of an adjacent molecule, since this intensity reversal is not observed upon detergent addition to aqueous PP solutions.[15] The $\gamma_{C_aC_m}$ mode is seen for all the P*a* complexes (Figure 5) at ~300 cm^{-1} and is unobscured by a vinyl bending mode, as it is for PP complexes. The pyrrole tilting band,

(38) Spiro, T. G.; Stong, J. D.; Stein, P. *J. Am. Chem. Soc. U.S.A.* **1979**, *101*, 2648.

however, is difficult to resolve from the flanking skeletal bands, while the $\gamma_{C_\beta S}$ band can be obscured by an overlapping band due to a Fermi resonance between ν_9, which produces the strong band at ~342 cm^{-1}, and $2x\nu_{35}$.[16,29] In some cases ($(ImH)_2Fe^{II}Pa$ and (2-MeImH)$Fe^{II}Pa$) the two bands in the 360–385-cm^{-1} region are resolved (Figure 5). The most plausible assignments are given in Table II.

Above the $\gamma_{C_\beta S}$ band, one finds a band at 414–418 cm^{-1}, assignable to vinyl in-plane bending, and then several bands between 440 and 530 cm^{-1} which are attributed to folding modes of the pyrrole rings. There are eight such modes, (two per pyrrole); in D_{4h} symmetry four of them occur in degenerate pairs (E_g), but the degeneracy can readily be lifted by the inequivalent substituents in P*a* or PP. As many as five bands in this region can be identified for $(ImH)_2Fe^{II}Pa$, if the aqueous and detergent spectra are interleaved (Figure 8). Two of these (504 and 488 cm^{-1}) line up with frequencies of the PP analogue (Table V), while a third band of the latter, at 426 cm^{-1}, is designated as a sixth pyrrole folding mode.[16] Confirming the pyrrole folding assignment of the 488-cm^{-1} band is its 6-cm^{-1} downshift upon formyl deuteration (Figure 10), since formyl and pyrrole out-of-plane deformations are expected to be coupled. It is interesting that the 488-cm^{-1} band also shifts down upon vinyl deuteration in PP.[16] Since the P*a* formyl group is on a different pyrrole from either of the PP vinyl groups, the mutual shifts imply that the mode is not localized on a particular pyrrole, but has significant contributions from at least two of them. Delocalization is also implicit in the spread of frequencies of the pyrrole folding modes. In addition to the 488-cm^{-1} band, the 507-cm^{-1} band, but not the 426-cm^{-1} band, shifts down on vinyl deuteration in $(ImH)_2Fe^{II}PP$. For the P*a* analogue the remaining pyrrole folding modes are too weak to determine formyl deuteration shifts, except for the 468-cm^{-1} band, which shows a curious 4-cm^{-1} upshift (Figure 10). Also the 299-cm^{-1} ($\gamma_{C_aC_m}$) and 343-cm^{-1} (ν_8) bands shift up by 2 cm^{-1}. These upshifts are not understood.

A depolarized band at 841 cm^{-1} in the RR spectrum of $(ImH)_2Fe^{II}PP$, which disappears on methine deuteration has been assigned to the E_g γ_{C_mH} mode.[16] A band near this frequency is seen for all the P*a* complexes (Table II). In addition $(ImH)_2Fe^{II}Pa$ shows an extra band at 833 cm^{-1} (Figure 8), which may be another γ_{C_mH} mode (A_{2u} or B_{2u} in D_{4h} symmetry). The IR spectrum of $ClFe^{III}Pa$ (Table V) shows a band at 838 cm^{-1}, which is probably the A_{2u} γ_{C_mH} mode.

Two Fe–axial ligand stretching modes can be identified in the heme *a* RR spectra shown in Figure 5. The 202-cm^{-1} band of $(ImH)_2Fe^{II}Pa$ coincides with the band of its PP analogue which has been assigned, on the basis of $ImH^{15}N^{34}$ and perdeuteration[35] shifts, to the Fe–$(ImH)_2$ symmetric stretch. The strong 211-cm^{-1} band of (2-MeImH)$Fe^{II}Pa$ is the Fe–2-MeImH stretch, identified via ligand perdeuteration[39] and ^{54}Fe shifts[40,41] in several (2-MeImH)Fe^{II} complexes at 205–220 cm^{-1}. The variability in frequency has been attributed to the effect of H bonding.[42] Nonpolar solvents, incapable of H bonding, give frequencies at the low end of the scale, while for aqueous solutions the frequency is 220 cm^{-1}. The frequency observed here for detergent solution, 211 cm^{-1}, which suggests slight H bonding within the micelles, is in line with frequencies reported for other (2-MeImH)Fe^{II} complexes in detergents.[34,41]

H. Cytochrome Oxidase. In Figure 16A,B the 4131-Å RR spectrum of cytochrome oxidase (cyt ox) in the oxidized form is compared with those of $(ImH)_2Fe^{III}Pa$ and $(Me_2SO)_2Fe^{III}Pa$, which were chosen as analogues for the cytochrome (cyt) *a* and a_3 sites (low- and high-spin), respectively. Figure 17A,B compares the 4545-Å RR spectrum of reduced cyt ox with those of $(ImH)_2Fe^{II}Pa$ and (2-MeImH)$Fe^{II}Pa$. These wavelengths gave maximal enhancement, in resonance with the (composite) B absorption bands. Similar comparisons have previously been reported,[2-11] but with the aid of the present heme *a* assignments, more definitive correlations can be made, as indicated in Table VII.

It should be noted that photoreduction of the oxidized enzyme by the incident laser beam has been found to occur in several studies,[4,5,8,9b] especially when stationary samples are excited. Our samples were always spun, and there is no evidence of subsidiary bands in the RR spectrum (Figure 16A) of oxidized cyt ox, which are clearly due to reduced heme *a*. In particular the strong sharp 1371-cm^{-1} band shows no 1358-cm^{-1} shoulder, as would be expected if heme *a* were being reduced. However, Babcock et al.[9b] have presented evidence that partial photoreduction can occur without development of a pronounced 1358-cm^{-1} shoulder but with the growth of strong new bands at 1612 and 1622 cm^{-1} when excited at 4067 Å. It is therefore possible that the 1618- and 1626-cm^{-1} bands observed in our oxidized cyt ox spectrum are due to partially photoreduced heme *a*, and the assignment of these modes (Table VII) to ν_{10} of cyt a_3 and $\nu_{C=C}$ of cyt *a* must be viewed as uncertain.

1. Formyl C=O Stretch. In the oxidized protein, the B band of the high-spin cyt a_3 is expected to be blue-shifted relative to the low-spin cyt *a*, and it has been suggested[9b,10] that excitation with the violet lines (4067 or 4131 Å) of the Kr^+ laser enhances the cyt a_3 modes more than those of cyt *a*. This is borne out when one examines, for example, the positions characteristic for the skeletal mode ν_3: 1478 and 1503 cm^{-1} for $[(Me_2SO)_2Fe^{III}Pa]^+$ and $[(ImH)_2Fe^{III}Pa]^+$. Cyt ox shows only a weak band at 1504 cm^{-1}, comparable in intensity to the band at 1500 cm^{-1}, which correlates with the weakly enhanced ν_{38x} of $(Me_2SO)_2Fe^{III}Pa$. Consequently, we agree with Babcock and co-workers[9b] that the 1676-cm^{-1} band is due to the formyl C=O stretch of cyt a_3, although both $[(Me_2SO)_2Fe^{III}Pa]^+$ and $[(ImH)_2Fe^{III}Pa]^+$ (in CH_2Cl_2) show $\nu_{C=O}$ at 1666 cm^{-1}. The reason for the 10-cm^{-1} upshift of this mode in the protein relative to $[(Me_2SO)_2Fe^{III}Pa]^+$ is uncertain. It is in the direction opposite that expected for H bonding, or any other influence which enhances electron delocalization into the C=O π^* orbital. A decrase in delocalization, accounting for the upshift, might be produced by the proximity of a negative charge or negatively oriented dipole in the protein.

The occurrence of a 1650-cm^{-1} band in the protein is intriguing, since this frequency is well removed from any feature of $[(Me_2SO)_2Fe^{III}Pa]^+$. We suggest that it arises from the coalescence of ν_{10} (expected at 1640 cm^{-1}) and $\nu_{C=O}$ of cyt *a*. This coalescence would be induced by a downshift of $\nu_{C=O}$, due to H bonding or other positive polarization, as is observed for $[(ImH)_2Fe^{III}Pa]^+$ in water (Figure 11). This interpretation implies that the cyt *a* formyl group is exposed to solvent or that it is near a positive charge or H-bond donor of the protein.

For the reduced protein, the 4545-Å RR spectrum appears to be dominated by cyt *a*, as judged (Figure 16) from the prominence of the bands at 1493, 1520, 1574, and 1588 cm^{-1}, all attributable to a low-spin Fe^{II} heme *a*, as well as the pair of bands at 1229 and 1251 cm^{-1}. However, the 1667-cm^{-1} band must arise from $\nu_{C=O}$ of cyt a_3; it is 7 cm^{-1} higher than the frequency observed for (2-MeImH)$Fe^{II}Pa$ in CH_2Cl_2 (Table I), paralleling the upshift seen in the oxidized form. No band is observed in the vicinity of 1644 cm^{-1}, the $\nu_{C=O}$ frequency for $(ImH)_2Fe^{II}Pa$ in Me_2SO. Babcock and Salmeen[4b] have suggested that the cyt *a* $\nu_{C=O}$ is not seen because the formyl group is twisted out of conjugation with the porphyrin ring. It is possible, however, that $\nu_{C=O}$ is shifted down under $\nu_{C=C}$ at 1624 cm^{-1}, as it is for $(ImH)_2Fe^{II}Pa$ in water. H bonding or other polarization effects could be responsible for the downshift, as suggested above for cyt *a* in the oxidized protein. The appearance of the ring–formyl stretch, at 1229 cm^{-1}, is quite similar to that of $(ImH)_2Fe^{II}Pa$ in detergent solution (Figure 17A). In water this band shifts down to 1220 cm^{-1} while in Me_2SO it shifts up to ~1240 cm^{-1} (see Figure 7). Consequently moderate H bonding is suggested. On the other hand the position of ν_{11}, which is also sensitive to H bonding, is the same, 1520 cm^{-1}, as for $(ImH)_2Fe^{II}Pa$ in Me_2SO. If the formyl conjugation were lost, ν_{11} would be expected to shift up, to ~1535 cm^{-1}, its frequency

(39) Kincaid, J.; Stein, P.; Spiro, T. G. *Proc. Natl. Acad. Sci. U.S.A.* **1979**, *76*, 549, 4156.
(40) Kitagawa, T.; Nagai, K.; Tsubaki, M. *FEBS Lett.* **1979**, *104*, 376.
(41) Hori, H.; Kitagawa, T. *J. Am. Chem. Soc.* **1980**, *102*, 3608–3613.
(42) Stein, P.; Mitchell, M.; Spiro, T. G. *J. Am. Chem. soc.* **1980**, *102*, 7795.

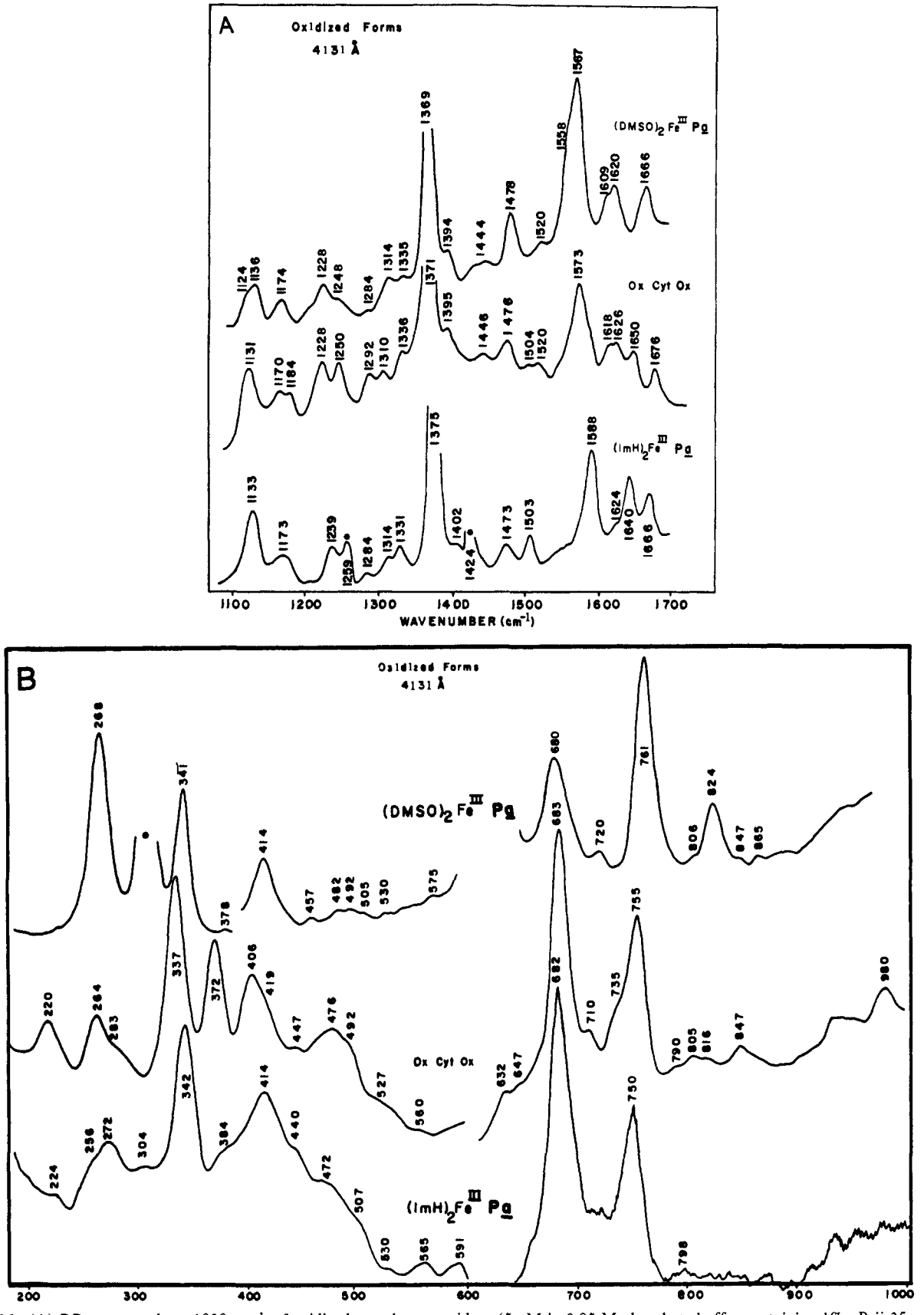

Figure 16. (A) RR spectra, above 1000 cm^{-1}, of oxidized cytochrome oxidase (5 μM in 0.05 M phosphate buffer containing 1%. Brij-35, pH 7.4) and of the cyt a_3 and a analogues $[(Me_2SO)_2Fe^{III}Pa]^+$ in Me_2SO, and $[(ImH)_2Fe^{III}Pa]^+$ in CH_2Cl_2 (20 μM heme). λ_0 = 4131 Å. Conditions: 70-mW laser power, 10 cm^{-1} slit width, 3 s/0.5 cm^{-1} intervals. (B) RR spectra below 1000 cm^{-1} as in Figure 16A, except $[(ImH)_2Fe^{III}Pa]^+$ was in H_2O.

for $(ImH)_2Fe^{III}PP$. Thus, the positions of $\nu_{C=O}$, ν_{C_b-CHO}, and ν_{11} give somewhat conflicting indications on the state of the formyl group; it is possible that there is both H bonding and some twisting out of the porphyrin plane.

2. Skeletal Frequencies. The frequencies assignable to ν_2 and ν_{10} (but note the uncertainty associated with ν_{10}, as discussed above) of cyt a_3 in the oxidized protein, 1573 and 1618 cm^{-1}, are 6 and 9 cm^{-1} higher than the $[(Me_2SO)_2Fe^{III}Pa]^+$ frequencies,

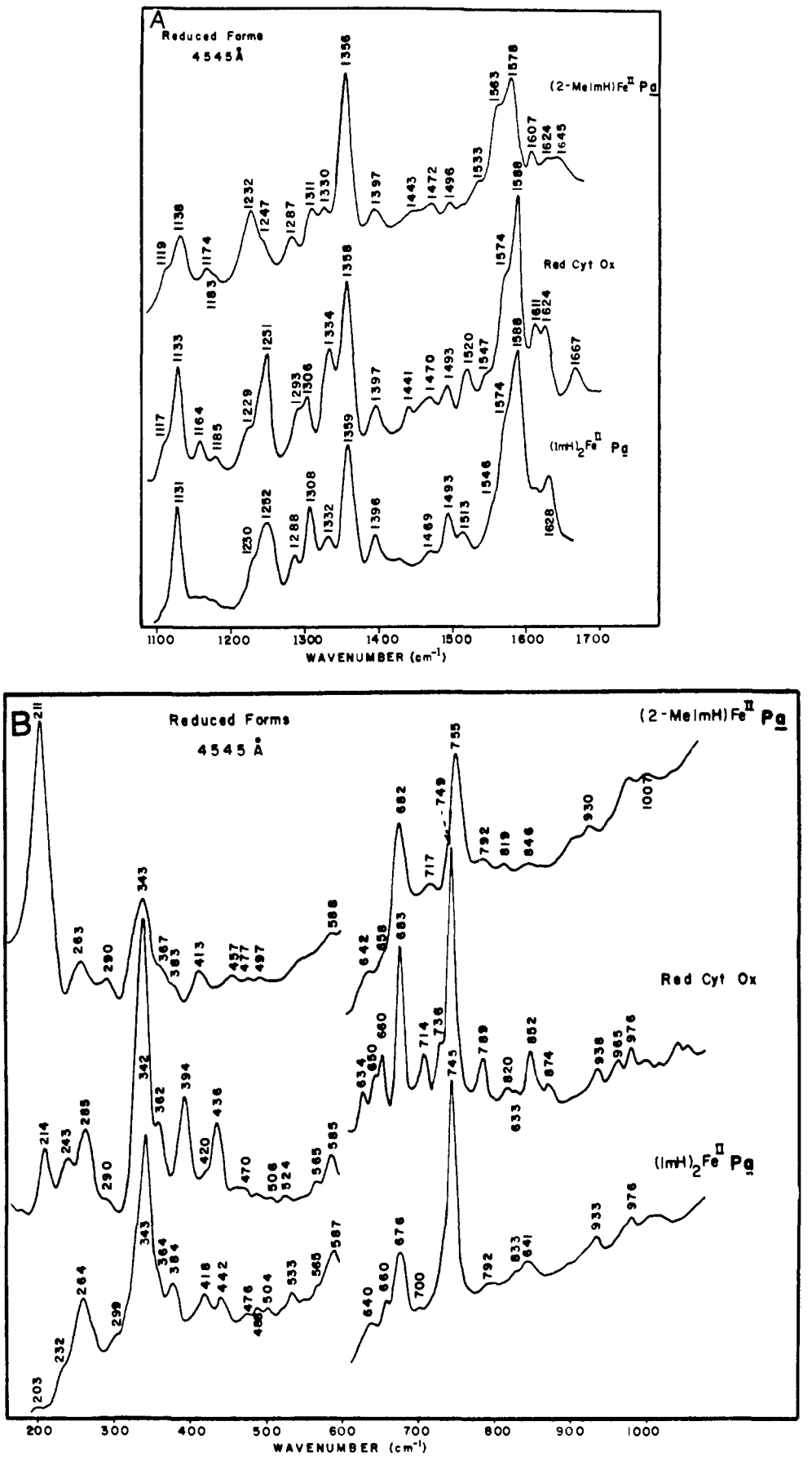

Figure 17. (A) RR spectra above 1000 cm^{-1} of reduced cytochrome oxidase and the analogues (2-MeImH)Fe^{II}P*a* and (ImH)$_2$Fe^{II}P*a*, both in Brij-35 (2%). Concentrations and conditions as in Figure 16A. (B) RR spectra below 1000 cm^{-1} as in Figure 17A.

Table VII. Raman Frequencies of Oxidized Cytochrome Oxidase and Models

	$[(ImH)_2$-$Fe^{III}Pa]^+$		cyt ox_{ox}		$[(Me_2SO)_2$-$Fe^{II}Pa]^+$	$(ImH)_2$-$Fe^{II}Pa$		cyt ox_{red}		(2-MeImH)-$Fe^{II}Pa$
ν_{CO}	1666		1676		1666	1644		1667		1660
$\nu_{CO\cdots H}$	1656					1628[b]				1645
		···	1650							
ν_{10}	1640									
			1618	···	1609	1620		1611	···	1607
$\nu_{C=C}$	1624	···	1626		1620	1623	···	1624	···	1624
ν_{37x}						1588	···	1588		1563
ν_{38x}						1574	···	1574		1533
ν_2	1588	···	1588							
			1573	···	1567	1593				1578
ν_{11}	1553		1520	···	1520	1513[b]	···	1520		
ν_{38y}	1540					1546	···	1547		1496
ν_3	1503	···	1504			1493	···	1493		1472
			1476	···	1478					
ν_{28}	1473		1446	···	1444	1469	···	1470		
								1441	···	1443
$\nu_{29/20}$	1402		1395	···	1394	1396	···	1397	···	1397
ν_4	1375		1371	···	1369	1359	···	1358		1356
$\delta_s{=}CH_2(2)$	1331		1336	···	1335	1332	···	1334		1330
ν_{21}	1314	···	1310	···	1314	1308	···	1306		1311
ν_{42}	1284	···	1292	···	1284	1288	···	1293	···	1287
$\nu_5 + \nu_9$			1250	···	1248	1252	···	1251	···	1247
ν_{C_bCHO}	1239		1228	···	1228	1230[b]	···	1229		1232
			1184					1185	···	1183
ν_{30}	1173	···	1170	···	1174	1168	···	1164		1174
$\nu_6 + \nu_8$	1133	···	1131		1136	1131	···	1133		1138
$\nu_{20} + \nu_{35}$						976	···	976		
								965		
ν_{46}						933	···	938		930
γ_{C_mH}			847	···	847	841		852	···	846
			816	···	824	833	···	833		
ν_6			805	···	806					819
ν_{32}	798	···	790			792	···	789	···	792
ν_{16}	750	···	755		761	745	···	749		755
ν_{47}			735					736		
				···	720	700			···	717
			710					714		
ν_7	682	···	683		680	676		683	···	682
			652			660	···	660		
δ_{CO}								650	···	658
			647			640	···	634		642
ν_{48}	591				575	587	···	585	···	588
ν_{49}	565	···	560			565	···	565		
pyr fold	530	···	527		530	533	···	524		
pyr fold	507					504	···	506		
pyr fold			492	···	492	488		470		497
pyr fold	472		476		482	478				477
pyr fold	440		447		457	442				457
$\delta_{C_bC_\alpha C(1)}$	414	···	406	···	414	418	···	420		413
γ_{C_bS}	384		372	···	378	384	···	394	···	383
$2\nu_{35}$						364	···	362	···	367
ν_8	342	···	337	···	341	343	···	342		343
$\gamma_{C_mC_a}$	304	···	283			299	···	290	···	290
ν_9	272	···	264	···	268					
pyr tilt	256					264	···	265	···	263
	224	···	220			232	···	243		
ν_{Fe-N}						203		214	···	211

implying a slightly contracted porphyrin core. The average C_t–N distance calculated from these frequencies, using the parameters in Table IV, is 2.04_5 Å for $[(Me_2SO)_2Fe^{III}Pa]^+$ (the crystallographically determined distance for $[(Me_2SO)_2Fe^{III}TPP]ClO_4$ is 2.045 Å[43]) and 2.02_8 for cyt a_3. (The ν_3 frequency, 1475 cm^{-1} in $(Me_2SO)_2Fe^{III}Pa$, should also increase, but does not appear to do so; the protein band is broad, however, and may contain a contribution from ν_{28} of cyt a, at 1473 cm^{-1} in $[(ImH)_2Fe^{III}Pa]^+$.) The slight decrease in C_t–N is plausibly associated with a lengthened bond to one of the axial ligands, which the recent EXAFS study by Powers et al.[13] has indicated to be a distant (2.60 Å) sulfur atom, probably belonging to a cysteine ligand of the antiferromagnetically coupled Cu^{2+}. The long bond would decrease the nonbonded interactions of the axial ligand with the pyrrole N atoms,[44] allowing the core to contract. The Fe–N(pyrrole) distance obtained from the EXAFS analysis,[13] 2.01 ± 0.03 Å, is within experimental error of the C_t–N distance given by the RR frequencies. This congruence implies that the Fe atom is close to being in the heme plane; otherwise the Fe–N(pyrrole) distance should exceed C_t–N significantly. The difference in the two distances, Δ, is just the square of the out-of-plane displacement, d, divided by the sum of the distances. If $d \simeq 0.5$ Å, as it typically is in five-coordinate hemes, then $\Delta \simeq 0.06$ Å, but if d is only ~0.2 Å, then Δ is ~0.01 Å, which is within the un-

(43) Mashiko, T.; Kastbern, M. E.; Spartalian, K.; Scheidt, W. R.; Reed, C. A. *J. Am. Chem. Soc.* **1975**, *97*, 2517.

(44) (a) Olafson, B. D.; Goddard, W. A. *Proc. Natl. Acad. Sci. U.S.A.* **1977**, *74*, 1315. (b) Warshel, A. *Ibid.* **1977**, *74*, 1789.

certainty range of the experimental values.

In the reduced protein a band is observed at 1611 cm^{-1}, which is probably ν_{10} of cyt a_3; it is 4 cm^{-1} higher than in (2-MeImH)Fe^{II}P*a*. This slight elevation of ν_{10} might be due to core contraction, or else to a decrease in porphyrin doming in the five-coordinate complex; negative deviations of several of the (2-MeImH)Fe^{II}PP skeletal frequencies from the C_t–N correlations have been attributed to doming.[15] In fact the ν_{10} frequency calculated for C_t–N = 2.044 Å (the crystallographic value for (2-MeImH)Fe^{II}TPP[19]) is 1611 cm^{-1}, the value observed in the protein RR spectrum. (The calculated value of ν_3, 1482 cm^{-1}, is higher than the 1470-cm^{-1} frequency observed in the protein, but this band is broad and may be dominated by ν_{28} (1469 cm^{-1}) of cyt *a*. Likewise the ν_2 region (1578 cm^{-1}) is obscured by cyt *a* bands.)

The remaining protein bands occur at positions expected (Table VII) on the basis of the analogue complexes, with minor exceptions. The ν_{30} frequency is slightly (3–4 cm^{-1}) lower in the protein; in PP complexes this mode is known to have a substantial contribution from ring–vinyl stretching. An additional band on the high-frequency side of ν_{30}, at 1184 cm^{-1}, shows up in the protein spectra. This mode is also seen as a shoulder in the (2-MeImH)Fe^{II}P*a* spectrum; its assignment is uncertain. The ν_{42} frequency, 1292 cm^{-1}, is appreciably higher (5–8 cm^{-1}) in the protein than in the analogues. This mode has a major contribution from C_m–H in-plane bending[30] and the frequency elevation suggests that the C_mH atoms are restrained by protein contacts. Likewise the out-of-plane γ_{C_m-H} frequency, 852 cm^{-1} is substantially (6–11 cm^{-1}) higher in the reduced protein (for which the band is quite prominent, Figure 16B), although in the oxidized protein the frequency (847 cm^{-1}) is normal. Since the major contributors to the reduced and oxidized protein spectra appear to be cyt *a* and cyt a_3, respectively, it may be inferred that the protein–methine contacts are more restrictive for cyt *a* than cyt a_3.

3. Low-Frequency Modes. The bands in the 600–900-cm^{-1} region assignable to in-plane deformation modes line up satisfactorily between protein and models (Table VII), with slight frequency shifts. Extra, unassigned bands are seen at 650–660 cm^{-1}, at 820–830 cm^{-1}, and at 965 cm^{-1}. An additional band at 735 cm^{-1} is suggested to arise from splitting of the ν_{47} E_u mode, the other component being at 710–714 cm^{-1}. The higher frequency component may be obscured by the strong ν_{16} (750 cm^{-1}) band in the analogue complexes.

The bands in the 430–535-cm^{-1} region, assigned to pyrrole folding, are weak in the protein spectra, except for the prominent 436-cm^{-1} band of cyt ox_{red}, which is much stronger and 6 cm^{-1} lower in frequency than its $(ImH)_2Fe^{II}$P*a* analogue. The vinyl bending mode, $\delta_{C_bC_aC_\beta}$, is 8 cm^{-1} lower in cyt ox_{ox} (406 cm^{-1}) than in either of the analogues, but this is not the case for cyt ox_{red}. Likewise, the cyt ox_{ox} bands assigned to γ_{C_bS} (372 cm^{-1}), ν_8 (337 cm^{-1}) and ν_9 (264 cm^{-1}) are all 4–6 cm^{-1} lower than the corresponding $[(Me_2SO)_2Fe^{III}Pa]^+$ bands. For cyt ox_{red}, the band assigned to γ_{C_bS}, 394 cm^{-1}, is 10 cm^{-1} higher than for $(ImH)_2Fe^{II}$P*a*, while ν_8 (342 cm^{-1}) is at its normal position (the position of ν_9 is obscured by the 265-cm^{-1} band assigned to pyrrole tilting).

Woodruff et al.[10] noted the discrepancy between cyt ox_{ox} and $(Me_2SO)_2Fe^{III}Pa]^+$ with respect to the band we have assigned to ν_8 and inferred that they arise from different vibrational modes. They further observed that the intensity of the cyt ox_{ox} low-frequency bands, when excited at 4131 Å, was greatly reduced upon protein reduction, or cyanide complexation, more than expected from the loss in resonance enhancement due to shifting of the B band. They noted a correspondence between the cyt ox_{ox} RR frequencies and those shown by "blue" copper proteins in the 250–450-cm^{-1} region and suggested that the cyt a_3 coupled Cu^{2+} ion might be responsible for the cyt ox_{ox} features. In our view, however, the correspondence between the low-frequency bands of cyt ox_{ox} and $[(Me_2SO)_2Fe^{III}Pa]^+$ is quite satisfactory; the 4–8-cm^{-1} downshifts are plausibly interpreted via a specific interaction of the heme a_3 peripheral substituents with the protein. Both ν_8 and ν_9 are calculated[30] to have major contributions from in-plane bending of the peripherial substituents, and of course γ_{C_bS} and $\delta_{C_bC_aC_\beta}$ involve the substituents explicitly. Intensity arguments are difficult to quantify because of the dependence of RR intensities on environmental effects, as evidenced, in the low-frequency region, by the marked intensity reversals noted upon heme *a* aggregation (see above). The cyt ox_{ox} intensity pattern is actually quite similar to that of $(Me_2SO)_2Fe^{III}Pa$, except that the 372-cm^{-1} γ_{C_bS} band is markedly intensified, presumably due to the same protein interaction responsible for its frequency shift. Likewise the upshifted 394-cm^{-1} γ_{C_bS} band of cyt ox_{red} is much stronger than the corresponding 384-cm^{-1} band of $(ImH)_2Fe^{II}$P*a*. The out-of-plane methine deformation, $\gamma_{C_aC_m}$ at ~290 cm^{-1}, seems to be downshifted in both forms of the protein, by ~10–20 cm^{-1} relative to the analogue complexes, but the bands are quite weak and their positions uncertain.

Finally, the prominent 214-cm^{-1} band of cyt ox_{red} can be assigned to the Fe–imidazole stretch of heme a_3, as has previously been noted.[11] The frequency is close to that observed for (2-MeImH)Fe^{II}P*a* in aqueous detergent and, as discussed above, is consistent with weak H bonding of the proximal imidazole, presumably to a protein acceptor.

Acknowledgment. We thank Dr. James Kincaid for the gift of a sample of 2-formyl, 4-vinyl heme. This work was supported by NIH Grant HL 12526.

Registry No. $(ImH)_2Fe^{III}$(P*a*), 85201-86-1; $(ImH)_2Fe^{III}$(PP), 78261-91-3; $(ImH)_2Fe^{II}$(P*a*), 63286-91-9; $(ImH)_2Fe^{II}$(PP), 20861-23-8; $ClFe^{III}$(P*a*), 19554-22-4; $ClFe^{III}$(PP), 16009-13-5; $(Me_2SO)_2Fe^{III}$(P*a*), 85248-64-2; $(Me_2SO)_2Fe^{III}$(PP), 85167-80-2; (2-MeImH)Fe^{II}(P*a*), 85167-81-3; (2-MeImH)Fe^{II}(PP), 70085-59-5; cytochrome oxidase, 9001-16-5.